Accommodation of Arabia-Eurasia convergence in the Zagros-Makran transfer zone, SE Iran: A transition between collision and subduction through a young deforming system

V. Regard, O. Bellier, J. -C. Thomas, M. R. Abbassi, J. Mercier, E. Shabanian, K. Feghhi, S. Soleymani

Accommodation of Arabia-Eurasia convergence in the Zagros-Makran transfer zone, SE Iran: A transition between collision and subduction through a young deforming system

V. Regard,[1] O. Bellier,[1] J.-C. Thomas,[2] M. R. Abbassi,[3] J. Mercier,[4] E. Shabanian,[3] K. Feghhi,[3] and S. Soleymani[3]

Received 29 October 2003; revised 28 April 2004; accepted 12 May 2004; published 29 July 2004.

[1] At Iranian longitude, the Arabian plate is moving northward relative to Eurasia (~20 mm yr^{-1} according to GPS). To the east, this relative motion is accommodated by northward subduction under the E-W Makran emerged accretionary prism. To the west, it is accommodated partly by the Zagros fold-and-thrust belt and partly by the Alborz/Kopet Dagh deforming zones further north. This work investigates the NNW striking transition zone that connects Zagros and Makran: the Minab-Zendan fault system. Satellite images, and structural and geomorphic field observations show a distributed deformation pattern covering a wide domain. Five north to NW trending major faults were identified. They exhibit evidence for late Quaternary reverse right-lateral slip, and correspond to two distinct fault systems: the western one transferring the Zagros deformation to the Makran prism, and the eastern one northward transferring the deformation to the Alborz/Kopet Dagh. Tectonic study and fault slip vector analyses indicate that two distinct tectonic regimes have occurred successively since the Miocene within a consistent regional NE trending compression: (1) an upper Miocene to Pliocene tectonic regime characterized by partitioned deformation, between reverse faulting and en echelon folding; (2) a NE trending σ_1 axis transpressional regime homogeneously affecting the region since upper Pliocene. The change is contemporaneous with major tectonic reorganization regionally recorded. Therefore this study provides evidence for active deformation that is not localized, but distributed across a wide zone. It accommodates the convergence and transfers it from collision to subduction by transpressional tectonics without any partitioning process in the present-day period. *INDEX TERMS:* 8122 Tectonophysics: Dynamics, gravity and tectonics; 8102 Tectonophysics: Continental contractional orogenic belts; 8105 Tectonophysics: Continental margins and sedimentary basins (1212); 8010 Structural Geology: Fractures and faults; 9320 Information Related to Geographic Region: Asia; *KEYWORDS:* Zagros, Makran, Arabia, Collision, Subduction, transpressional, partitioning, active tectonics. **Citation:** Regard, V., O. Bellier, J.-C. Thomas, M. R. Abbassi, J. Mercier, E. Shabanian, K. Feghhi, and S. Soleymani (2004), Accommodation of Arabia-Eurasia convergence in the Zagros-Makran transfer zone, SE Iran: A transition between collision and subduction through a young deforming system, *Tectonics*, *23*, TC4007, doi:10.1029/2003TC001599.

1. Introduction

[2] Iran is located within the convergence zone between the Arabian and Eurasian plates. The eulerian pole for this motion is located near the Libyan coast [*McClusky et al.*, 2000, 2003; *Vernant et al.*, 2004], and the convergence velocity increases from the Bitlis collision zone to the Makran. Off the Hormoz Strait (26.5°N; 56.5°E), the Arabia-Eurasia convergence is trending north to NNE (Figure 1). Its estimated velocity ranges from 23 mm yr^{-1} (according to local GPS network [*Bayer et al.*, 2002]) to 35 mm yr^{-1} (according to the NUVEL-1 model [*DeMets et al.*, 1990]). The most reliable values for the convergence vector are provided by recent GPS studies at the Arabian plate scale and are about 25 mm yr^{-1} in a direction N10°E [*McClusky et al.*, 2003; *Vernant et al.*, 2004] (Table 1).

[3] The Zagros chain is a fold-and-thrust belt within the Arabian plate. Its average strike is NW, and the transversal NE trending shortening rate increases from NW to SE and reaches about 10 mm yr^{-1} near its southeastern edge [*Tatar et al.*, 2002; *Vernant et al.*, 2004]. To the east, the E-W striking Makran belt is the emergent portion of an accretionary prism resulting from the subduction of the Oman Gulf oceanic lithosphere (which forms part of the Arabian plate) beneath Iran [*Byrne et al.*, 1992; *McCall*, 1997; *Kopp et al.*, 2000]. A NNW trending deformation zone, the oblique reverse-dextral Minab-Zendan fault

[1]Centre Européen de Recherche et d'Enseignement en Géosciences de l'Environnement (CEREGE), UMR CNRS 6635, University Aix Marseille III, Aix en Provence, France.
[2]Laboratoire de Géophysique Interne et Tectonophysique (LGIT), UMR CNRS 5557, Grenoble, France.
[3]International Institute for Earthquake Engineering and Seismology (IIEES), Tehran, Iran.
[4]OrsayTerre, UMR CNRS 8616, University Paris XI, Paris, France.

0278-7407/04/2003TC001599

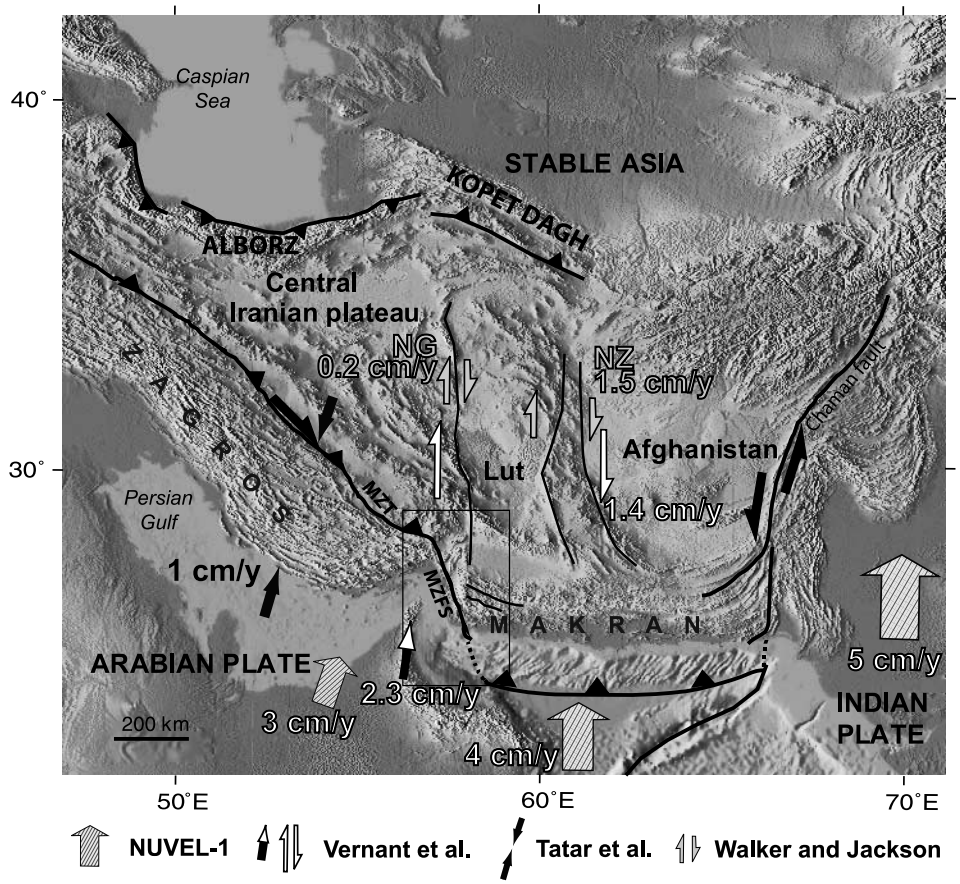

Figure 1. Geodynamic setting of Iran and adjacent areas. The main geodynamic structures are indicated; convergence velocities and deformation rates are indicated after the NUVEL-1 model [*DeMets et al.*, 1990], GPS studies [*Tatar et al.*, 2002; *Vernant et al.*, 2004] and tectonic work [*Walker and Jackson*, 2002]. The study area is indicated by an open rectangle. Abbreviations are as follows: MZT, Main Zagros Thrust; MZFS, Minab-Zendan fault system; NG, Nayband-Gowk fault system; NZ, Neh-Zahedan fault system.

system, connects the Western Makran and the Eastern Zagros deformation zones (Figure 2).

[4] Back in the Mesozoic, the Neotethyan Ocean was subducting to the north, under the Iranian and Afghan microplates (Figure 3a). In principle, once this closed, the geometry could have developed as in Figure 3b, but it did not because most of the deformation is taken up further north in the Alborz [*Allen et al.*, 2003a; *Vernant et al.*, 2004]. This implies that part of the convergence accommodated north of the central Iranian plateau must be transmitted to the Makran, without any E-W motion of the Central Iranian Plateau (i.e., with no extrusion, as could be reported with this kind of geometry; see *Jackson et al.* [1995] and *Bonini et al.* [2003]), through the north trending strike-slip Nayband-Gowk and Neh-Zahedan fault systems (Figure 3c).

[5] Taking into account its location at the plate boundary scale and its NNW trend, which is oblique to the direction of convergence, the Minab-Zendan fault system could have two major roles at a lithospheric scale: (1) to accommodate the plate convergence obliquity; and/or (2) to transform the Zagros collision process into the Makran subduction.

1.1. Seismicity and Expected Fault Activity

[6] The seismicity of the study area shows shallow earthquakes mainly located within the Zagros, and near

Table 1. Arabia-Eurasia Convergence Vector at Latitude 27°N, Longitude 57°E, After Different Models for the Arabian Plate Motion With Respect to the Eurasian Plate Motion

	DeMets et al. [1990]	*Sella et al.* [2002]	*McClusky et al.* [2003]	*Vernant et al.* [2004]
Azimuth, °N	6.6	6.4	9.7	11.2
Convergence rate, mm yr^{-1}	34.7	24.2	25.1	25.4

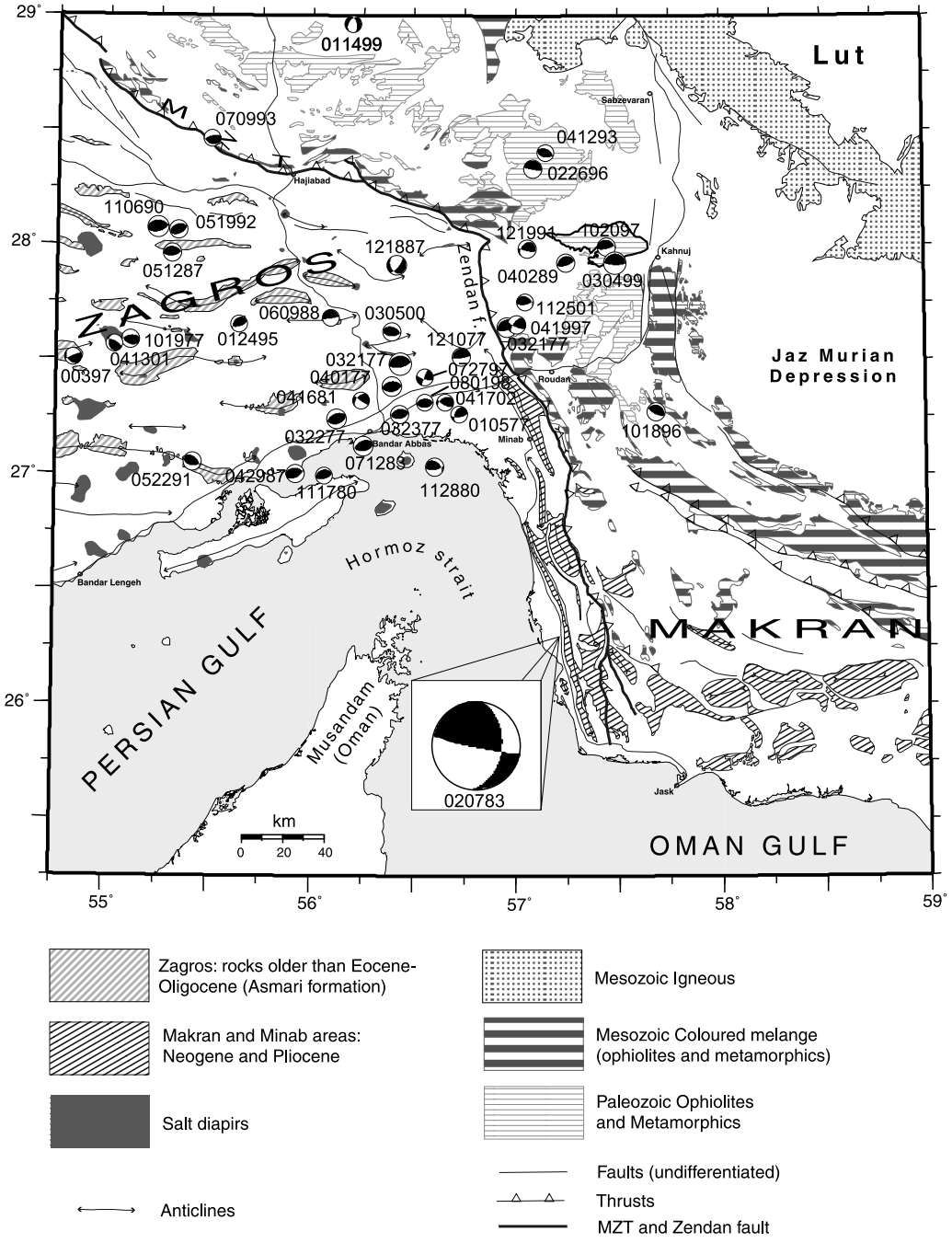

Figure 2. Structural map of the Zagros-Makran transition zone, modified after the 1:2,500,000 geological map of Iran. The Zendan fault trace is modified after this work (see hereafter). "Beach balls" represent Harvard CMT fault mechanisms for the period 1976–2002 (the date is mentioned mmddyy), the only one clearly related to the Minab-Zendan fault zone is enlarged. For clarity, rocks younger than Oligocene have not been drawn in the Zagros.

the northwestern termination of the Makran (Figure 2). Seismicity as recorded by global seismic networks and historical seismicity [*Berberian*, 1981; *Ambraseys and Melville*, 1982] (see also USGS National Earthquake Information Center catalog, available at http://neic.usgs.gov/neis/epic/epic.html, 2002), indicates a relatively low level of seismic activity in the deformation zone, whereas previous studies suggested major active structures along it [*Berberian*, 1981, 1995]. Moreover, if the entire convergence rate accommodated to the west by the Zagros fold-and-thrust belt is transmitted to the Makran wedge through the transform zone, the latter could undergo high slip rates,

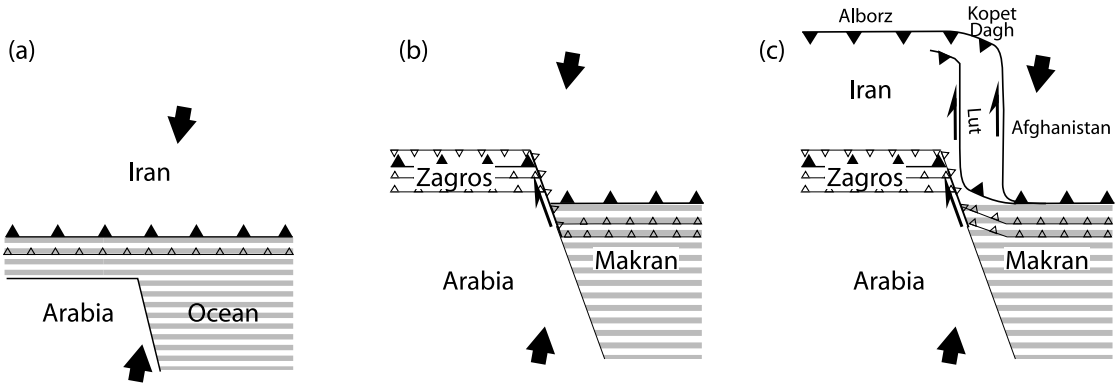

Figure 3. Simple scenario for the development of a transition between subduction and collision like the Zagros-Makran one. (a) At the beginning, the ocean is gently subducting under the continent to the north, until the closure of the ocean. (b) Then the collision begins, inducing a strike-slip fault. (c) The Zagros-Makran case is a little more complicated since the convergence vector is oblique to the Zagros and Makran structures and to the faults running northward. There are also others places for the accommodation of the Arabia-Eurasia convergence such as the Kopet Dagh to the NE of Iran.

as high as the 10 mm yr^{-1} Zagros shortening rate indicated previously. Only one large earthquake (M_w = 5.9; 2 July 1983; latitude, 26.3°N; longitude, 57.2°E; Figure 2) recorded by global seismic networks highlights the activity of the present day kinematics of the studied area. The focal mechanism provided by the Harvard Centroid-Moment Tensor (CMT) database gives evidence for a N05°E trending (for a dip of 42°E) focal plane [*Dziewonski et al.*, 1981; Harvard University Moment Tensor catalog (CMT Project) and data set available at http://www.seismology.harvard.edu/CMTsearch.html), consistent with the regional orientation of the structures. In addition, this focal mechanism suggests transpressional deformation is acting within the study area, i.e., mainly dextral strike-slip faulting with a slight reverse component, consistent with the NE trending *P* axis. The relative lack of seismicity at present may indicate aseismic deformation or accommodation of the deformation by major earthquakes separated by long quiescence intervals. Conversely, high seismicity in Zagros might be due to the presence of thick salt layers allowing distribution of deformation over a wide area [*Koyi et al.*, 2000].

[7] To complement the previous analyses and to understand this discrepancy between the low seismicity and the expected high lithospheric scale deformation rate, it is therefore crucial to determine the geometry and kinematics of the Zagros-Makran transfer zone. Another aim is to determine whether the deformation is localized on a single fault, or distributed on several distinct structures. In the latter case, it is important to check if the convergence is accommodated by strain partitioning, e.g., onto parallel pure dip-slip and pure strike-slip faults. Partitioning mechanisms have been previously described within subduction zones associated with oblique convergence, the earthquake slip vectors being commonly normal and parallel to the trench, oblique with respect to the predicted plate motion vectors. Consequently, relative plate motion along such convergent margins is partitioned into dip-slip displacements along the subduction plane and deformation within the overriding plate [*Fitch*, 1972; *McCaffrey*, 1992; *Bellier and Sébrier*, 1995]. The overriding plate deformation commonly corresponds to a shear component that is localized on trench-parallel, strike-slip fault zones. Similarly, partitioning was documented within intracontinental oblique convergence domains [*Gaudemer et al.*, 1995; *Ward and Valensise*, 1996], where deformation is accommodated by parallel structures, i.e., dip-slip thrusts accommodating the normal convergence component and strike-slip faults accommodating the transcurrent component. In continental deformation, the partitioning process seems to depend on the existence and location at depth of a ductile layer [*Richard and Cobbold*, 1990].

1.2. Overview

[8] The focus of the current study is twofold: (1) to characterize the active deformation pattern and to localize the high seismic potential zones, on the basis of tectonic and geomorphic field observations, complemented with SPOT satellite image and aerial photograph analysis, and (2) to determine the Quaternary to present-day state of stress acting within and around the Zagros-Makran transfer zone by inversion of both geologically and seismically determined slip vectors on minor and major faults within the zone. The possible occurrence of strain partitioning will be examined looking at the temporal faulting relationships and slip compatibility within a uniform regional stress field.

2. Geological Setting

[9] As mentioned above, the NW trending Minab-Zendan fault system connects the Zagros fold-and-thrust belt to the Makran prism. The Zagros is a fold-and-thrust belt affecting a roughly 6–15-km-thick sedimentary pile that overlies a Precambrian metamorphic basement corresponding to the northern extension of the Arabian shield [*McCall et al.*, 1985; *McCall*, 1997]. It is generally agreed that Iran was

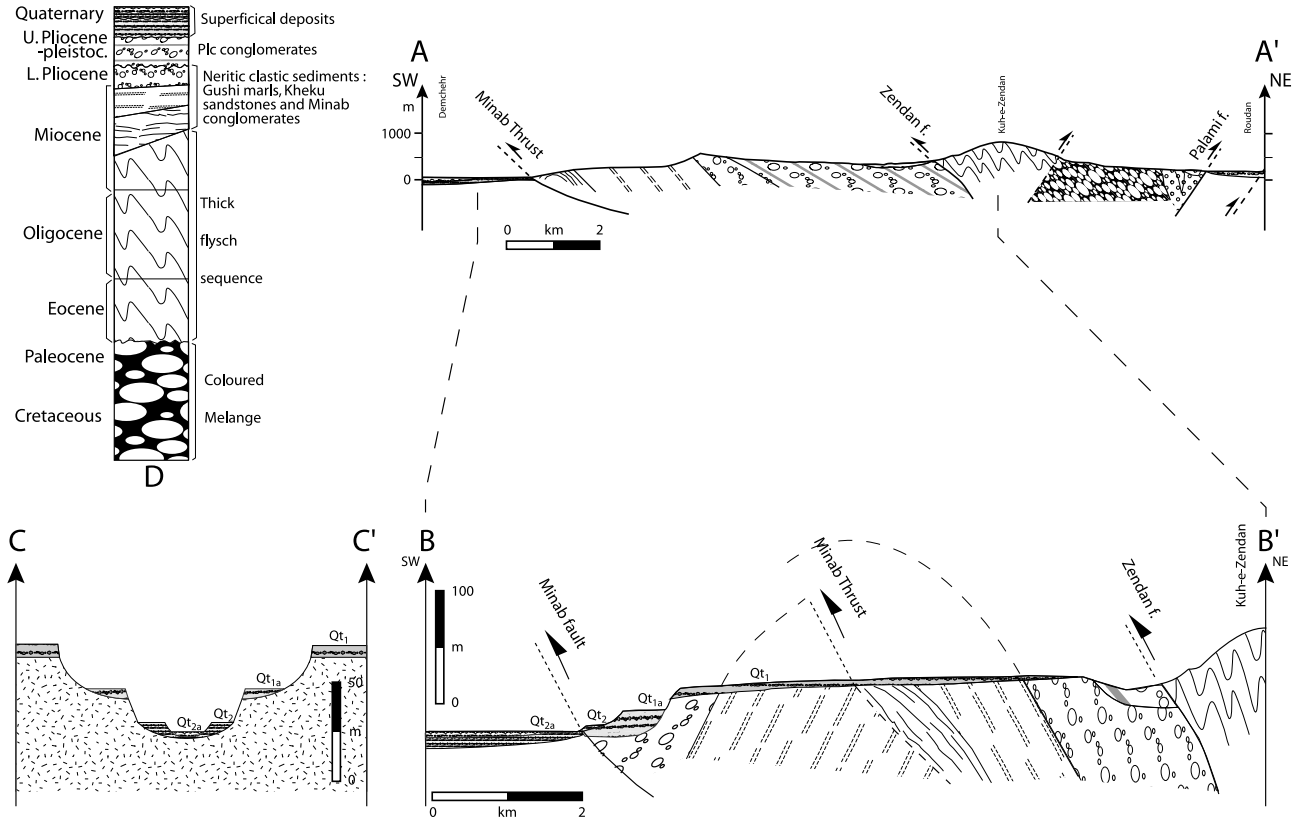

Figure 4. AA′, cross section across the Minab fold and Zendan range (see Figure 5). No vertical exaggeration. BB′, schematic cross section along the road from Bandar Abbas to Rudan (see Figure 5), with vertical exaggeration to show the relationship between the different pediments and terraces. CC′, schematic cross section perpendicular to BB′ to show the relationships between the different terraces. D, stratigraphic sequence of the Minab area, including Quaternary terraces, modified after *McCall* [1997] (with permission from *Journal of Asian Sciences*).

formed by the northeast extension of the Arabian platform in Paleozoic times. Its sedimentary cover is divided into three successive sequences: Precambrian to lowermost Cambrian shallow water platform deposits with thick evaporitic layers at the base; a Carboniferous to Cretaceous carbonate platform sequence [e.g., *O'Brien*, 1957; *Faure-Muret and Choubert*, 1971; *Ala*, 1974; *Colman-Sadd*, 1978; *Farhoudi*, 1978]; and uppermost Cretaceous to Recent synorogenic deposits which consist of interbedded platform carbonates and siliclastic sediments [*Alavi*, 1994]. The Zagros is built of this highly deformed sedimentary cover, folding over blind thrusts in the southwestern part and thrusting in the northeastern part. Balanced cross sections indicate 49 km of NE trending shortening since 5 Ma [*Blanc et al.*, 2003], in agreement with the ~50–70 km shortening estimate predicted across this part of the Zagros from the right-lateral offset of the Main Recent fault [*Talebian and Jackson*, 2002]. The cumulative shortening reported by *Blanc et al.* [2003] yields a NE trending shortening rate of 10 mm yr^{-1} that is consistent with the present-day shortening rate across the central Zagros of ~10 mm yr^{-1}, recently calculated by *Tatar et al.* [2002] on the basis of GPS measurements.

[10] The Makran is an accretionary wedge active since the late Oligocene [*Harms et al.*, 1984] and filled by detrital sediments coming from the Himalayan belt and deposited in the Oman Gulf [*Garzanti et al.*, 1996; *Fruehn et al.*, 1997; *Kopp et al.*, 2000]. Its mean elevation is about 1500 m and its across-strike width is 400–600 km [*Byrne et al.*, 1992]. The front of the wedge propagates seaward with a mean estimated rate of about 10 mm yr^{-1} [*White*, 1982]. The wide geographical extension and the high elevation of the wedge, as well as the thick sedimentary column at the wedge deformation front, probably result from the low angle of dip (about 5°N) of the subduction plane [*Jacob and Quittmeyer*, 1979; *Byrne et al.*, 1992; *Carbon*, 1996; *Kopp et al.*, 2000]. The northern boundary of the Makran wedge is abruptly marked by the wide E-W Jaz Murian depression [*McCall and Kidd*, 1982; *Boulin*, 1991; *McCall*, 1997].

[11] The Zagros-Makran transfer zone is a deformation zone affecting the Zagros to the west and Makran formations to the east (Figure 2) [*Kadjar et al.*, 1976, 1978; *McCall et al.*, 1985; *McCall*, 1997]. In the study area, the pre-Eocene formations (hereafter referred to as basement) are formed by Paleozoic rocks initially metamorphosed in pre-Jurassic times, Mesozoic to Paleocene platform

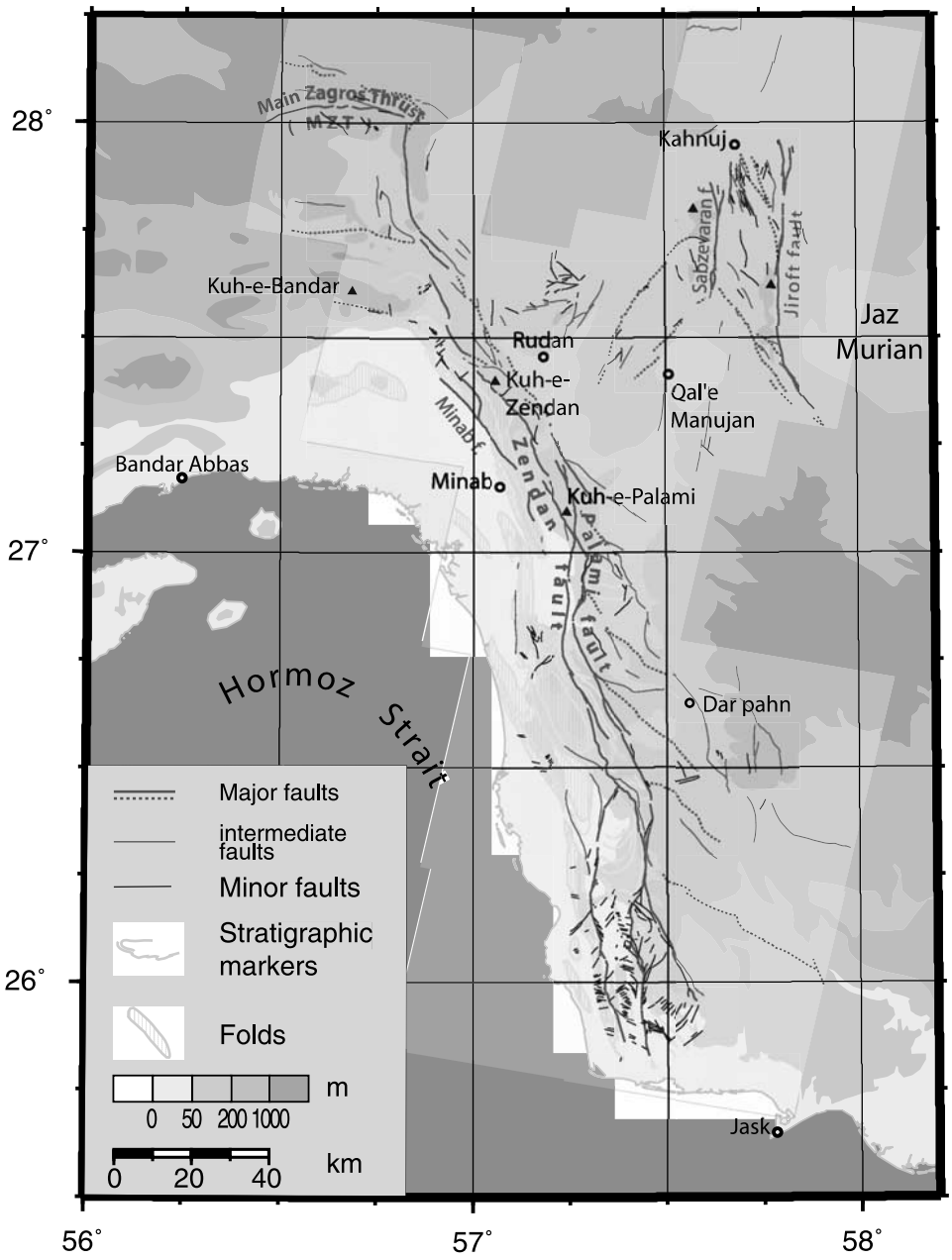

Figure 5. Structural and tectonic map drawn after SPOT satellite images. Major faults are active since they crosscut Quaternary deposits. When their activity is not verified they appear with a dotted line. Intermediate and minor faults are not clearly active. Their relative importance is based on their associated relief and their length. Stratigraphic markers are stratigraphic layers that can be easily followed on satellite images to pick out the deformed structures. Fold traces are the contour of fold-forming rocks. See color version of this figure at back of this issue.

sediments and ophiolitic suites. Several mafic/ultramafic complexes are evidence of Early Cretaceous and early Paleocene ophiolites associated with Upper Cretaceous and Paleocene platform deposits. The Upper Cretaceous-early Paleocene "colored melange" complex crops out widely within the wedge. It is made of ophiolites (pillow basalts, serpentinized ultrabasics…) mixed with conglomerates, reef limestones, distal turbidites, radiolarites and pelagic sediments. It is unconformably overlain by a ~10,000 m thick sequence of Eocene to Miocene flysch. These flysch experienced some significant movements especially during the Oligocene at the time the area underwent a major uplift [*Ricou et al.*, 1977]. Flysch sedimentation was followed by the deposition of early Miocene

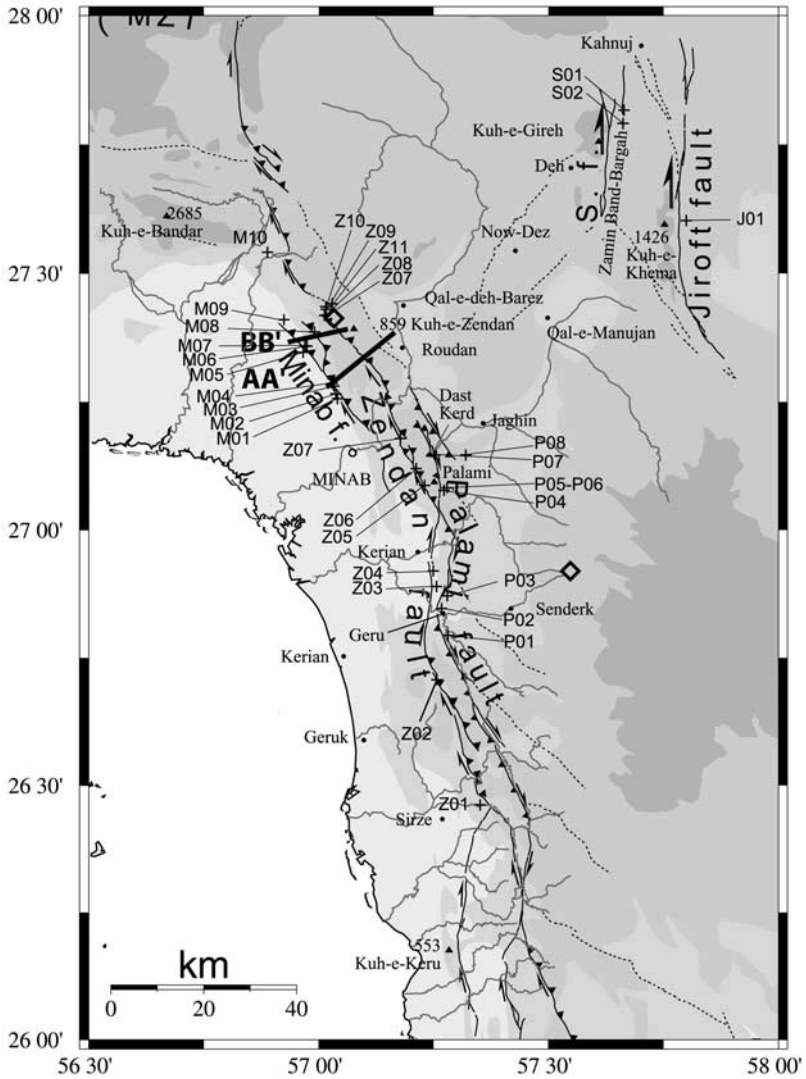

Figure 6. Map of the active faults, showing their motion, and location of cross sections of Figure 4; site striation measurements are indicated. Diamonds are locations of folds studied by *Delaunay et al.* [2002]. Note that the N160°E trending segments are transpressive while north trending ones are pure strike-slip faults. See Figure 5 for general legend.

intertidal and evaporitic facies sediment (see stratigraphic sequence, Figure 4) [*McCall*, 1997]. These deposits are separated by normal faults from middle-upper Miocene up to early Pliocene sediments deposited within the western, coastal, part of the study zone. These series, from bottom to top, consist of lagoonal pelagic gypsiferous marls (middle Miocene, Gushi marls, Figure 4), a sequence of deltaic and inshore sandstones and conglomerates with littoral aeolian and beach rock limestones near the coast (upper Miocene, Kheku sandstones) and an upper deltaic and fluviatile conglomerate (early Pliocene, Minab conglomerate). They constitute the Minab formation. This continental fluvial conglomerate is unconformably overlain by an upper Pliocene thick and coarse conglomerate (Plc on the map of *McCall et al.* [1985], whose age is estimated by cross-correlations) (Figures 1 and 4). This partly correlates laterally to the Plio-Pleistocene 4000-m-thick Palami conglomerate, which corresponds to the filling of intramontane basins, currently in the eastern part of the deformation zone. This large sediment supply probably testifies, as suggested by the geographic locations and shapes of these basins (within the chain), to the climactic uplift at the end of the late Neogene tectonism [*McCall et al.*, 1985; *McCall*, 1997], even if the intensity of this phenomenon could also have been increased by the climatic change invoked by *Zhang Peizhen et al.* [2001].

[12] All the formations described above have been intensively folded and uplifted in the area west of the Zendan range region. Since the Pleistocene, erosion of the resulting relief has produced piedmont spreading deposits at the foot of the range relief. These constitute the youngest formations, made of a series of Quaternary alluvial and colluvial

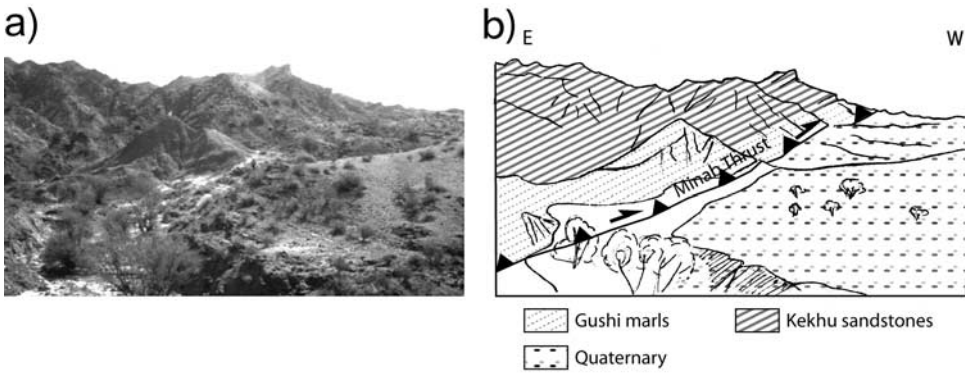

Figure 7. (a) South facing view of site M04 (Demchehr). (b) Interpretative drawing showing the trace of the Minab thrust. Quaternary corresponds to a terrace contemporaneous with the high pediment Qt_1.

sandy conglomerate deposits. Their succession corresponds to a Quaternary morphoclimatic sequence previously described by *Dufaure et al.* [1978; see also *Dufaure*, 1984; *McCall et al.*, 1985] corresponding to successive emplacements of pediments and alluvial fans which skirt the western piedmont of the Zendan range (Figure 3), the sequence of which we summarize as follows (dating is available from *Regard* [2003]): (1) a primitive pediment, produced during a middle Pleistocene wet episode as a result of the dissection of formerly produced folds; it is labeled Qt_1 in the Minab quadrangle of *McCall et al.* [1985] (see Figure 4); (2) a second generation of pediment (Qt_{1a}, Figure 4) dated from the early upper Pleistocene [*Dufaure et al.*, 1978] and corresponding mainly to coarse anastomosed alluvial terraces; (3) depositional phases corresponding to two upper Pleistocene (Qt_2) and Holocene (Qt_{2a}) generations of alluvial fan deposits. They are made of a poorly consolidated fanglomerate comprising coarse debris (mainly cobbles and abraded boulders) interbedded with silt and sand levels. On the Qt_2 fan surfaces, an epi-Palaeolithic (or Mesolithic) industry has been sampled [*Regard*, 2003; C. Thibault, unpublished data, 1977]. These two generations of well-preserved fans can be correlated with alluvial terraces recognized within the Zendan range and with alluvial fans observed within the Rudan and Jaz Murian depressions, particularly at the eastern slopes of the Zendan range and of the Sabzevaran and Jiroft horsts (Figures 4 and 5).

3. Tectonic Framework

[13] The studied region has been affected by several phases of deformation. The pre-Eocene and Oligocene phases seem mainly characterized by regional uplift processes [*Ricou et al.*, 1977], while the major folding event occurred during the late Neogene. Throughout the study area, an extensional event, occurring before the fold-and-thrust deformation, is indicated by the presence of normal faults tilted by the folding. However, the Jaz Murian depression seems to have been developed mainly during the upper Pliocene as a forearc basin [*McCall and Kidd*, 1982; *McCall*, 1997], whereas, in the Zagros-Makran transfer zone, the late Neogene tectonic regime corresponds to the westward propagation of folds and thrusts from the Zendan fault. Near Minab, the Zendan fault constitutes a boundary between the Makran, to the east, and the Mio-Pliocene molassic series, typical of the Zagros, to the west. This molassic series is folded and sheared, resulting in en echelon arranged folds with roughly the same orientation as the Zendan fault (Figure 5). This en echelon arrangement suggests a right-lateral component for the Minab-Zendan fold-and-thrust belt.

[14] West of the Zendan fault, the Quaternary pediments and fans unconformably overlie the folds affecting the late Miocene deposits. This indicates that the major phase of folding occurred after the late Miocene-early Pliocene and before the Quaternary. The coarsening up nature of the Pliocene Plc conglomerates argues for synsedimentary tectonic activity. The presence and thickness of Palami conglomerate probably reflects a climactic uplift at the end of the late Neogene tectonism. It could be the result of climate change and/or natural progradation of localized drainage systems over time. However, the thickness of the deposits (thousands of meters) and their location in the vicinity of major faults, suggest that the main active phenomenon is related to uplift, even if climate changes and/or drainage system progradation probably contribute to increase the deposited sediment volume. Unlike the Minab conglomerate, the upper Pliocene conglomerate (Plc and Palami conglomerate) is not (or is only very slightly) involved in regional large-wavelength folds of the Minab-Zendan fold-and-thrust belt. It is mainly locally folded by short wavelength (of the order of 2–5 km) drag folds close to the major faults.

[15] The emplacement of Quaternary pediments corresponds to a period of local uplift mainly realized between the formation of the old (Qt_1) and young (Qt_{1a}) pediments. Quaternary pediments as well as recent fans (Qt_2) are affected and offset by major faults implying that Quaternary tectonism is mainly characterized by faulting, the major folds having formed previously within the late Neogene. The major faults exhibit vertical and right-lateral offsets of geomorphic features (streams, late Quaternary alluvial fans,

Table 2. Results of Stress Tensor Inversions From Fault Slip Vector Data (Striations on Fault Planes)[a]

					σ_1		σ_2		σ_3	
	Age Lithology	Longitude	Latitude	R	Direction	Plunge	Direction	Plunge	Direction	Plunge
					NE-SW Compression					
Minab fault zone										
M01*	Kh	27.256	57.041	0.37	50	0	140	0	317	90
M02*	Q	27.265	57.038	0.70	52	0	142	0	320	90
M04*	Kh	27.285	57.030	0.79	220	0	130	0	311	90
M05	Qt_{1a}	27.345	56.967	0.84	229	11	320	4	69	78
M06	Qt_2	27.357	56.975	0.80	225	5	315	1	53	85
M07	Qt_{1a}	27.358	56.971	0.87	218	10	308	0	38	80
M08	Gu-Kh	27.385	56.991	0.77	40	14	308	9	187	74
M09	Qt_{1a}	27.409	56.926	0.70	42	18	132	1	225	72
Zendan fault zone										
Z01	Gu	26.465	57.352	0.32	236	10	327	8	94	78
Z02	Q/BR	26.708	57.258	0.49	250	3	340	10	144	79
Z03	Fy	26.890	57.257	0.59	209	1	118	55	299	35
Z04	Gu	26.920	57.250	0.88	222	5	130	24	322	65
Z05	Pal/Plc	27.087	57.231	0.94	242	2	150	40	335	50
Z06	Q	27.119	57.213	0.48	242	10	33	3	79	79
Z07	Gu-Kh	27.178	57.178	0.55	228	11	138	1	41	79
Z08*	Plc	27.417	57.013	0.69	58	0	148	0	324	90
Z09	Q	27.417	57.013	0.32	214	15	37	75	304	1
Z11	Gu/Fy	27.434	57.016	0.81	213	0	303	45	123	45
Z12*	BR	27.440	57.030	0.57	223	0	133	0	314	90
Palami										
P01	Fy	26.794	57.282	0.79	57	10	154	34	313	54
P03*	Plc	26.872	57.280	0.94	203	0	11	89	293	1
P03	Plc	26.872	57.280	0.84	220	2	129	28	313	62
P04*	Qt_{1a}	27.077	57.273	0.94	52	0	142	1	322	89
P06	Gu/Q	27.082	57.279	0.90	225	1	134	21	317	69
P07	Plc	27.146	57.254	0.95	42	15	140	25	284	60
Sabzevaran										
S02	BR	27.789	57.655	0.84	46	2	313	62	137	28
Fisher					227.1	1.0 (4.8°)	135.7	50.8 (39.9°)	315.3	85.6 (11.5°)
MFP				0.65	44	4	135	6	279	83
PPF				0.88	49	0	319	2	145	88
					E-W Compression					
M01*	Kh	27.256	57.041	0.96	75	0	165	1	344	89
M03	Kh	27.280	57.034	0.05	261	27	171	0	81	63
M04*	Kh	27.285	57.030	0.92	78	0	168	0	345	90
Z03*	Fy	26.890	57.257	0.12	70	0	160	0	312	90
Z05	Pal/Plc	27.087	57.231	0.85	274	2	184	19	11	71
Z07*	Gu/Kh	27.178	57.178	0.55	99	0	189	0	337	90
Z08*	Plc	27.417	57.013	0.69	81	0	171	0	338	90
Z11*	Gu/Fy	27.434	57.016	0.95	83	0	173	1	351	89
P02	Fy	26.847	57.267	0.77	259	14	161	31	10	56
P07*	Plc	27.146	57.254	0.23	257	12	167	1	70	78
P08*	Plc	27.146	57.320	0.43	103	0	193	0	331	90
S01*	BR	27.815	57.657	0.48	75	0	165	0	328	90
S01*	BR	27.815	57.657	0.69	98	0	188	0	345	90
S02*	BR	27.789	57.655	0.95	83	0	175	89	353	1
J01	BR	27.601	57.800	0.48	261	15	77	75	171	1
Fisher					263.3	5.3 (5.9°)	165.3	12.8 (23.6°)	28.3	81.8 (17.3°)
MFP				0.87	83	1	175	55	353	35
					N-S Compression					
M03*	Kh	27.280	57.034	0.96	179	0	89	0	272	90
M06*	Qt_2	27.357	56.975	0.85	180	0	90	0	279	90
M10	Plc	27.540	56.889	0.75	342	14	210	69	76	15
Z01	Gu	26.465	57.352	0.42	345	9	75	2	178	80
Z05	Pal/Plc	27.087	57.231	0.93	15	9	116	52	278	37
Z09*	Q	27.417	57.013	0.61	193	0	103	0	297	90
Z10*	Kh	27.429	57.017	0.92	184	0	94	0	278	90
P01	Fy	26.794	57.282	0.86	342	1	252	2	105	88
Fisher					0.0	4.5 (10.1°)			271.6	58.8 (30.8°)

Table 2. (continued)

					σ_1		σ_2		σ_3	
	Age Lithology	Longitude	Latitude	R	Direction	Plunge	Direction	Plunge	Direction	Plunge
					Extension					
Z05	Pal/Plc	27.087	57.231	0.36	215	64	35	26	125	0
Z11	Gu/Fy	27.434	57.016	0.71	145	73	344	16	253	5
S01*	BR	27.815	57.657	0.01	50	0	225	90	320	0

[a]Inversion results include the orientation (azimuth and plunge) of the principal stress axes of a stress tensor as well as a "stress ratio" $R = (\sigma_2 - \sigma_1)/(\sigma_3 - \sigma_1)$. Principal stress axes, σ_1, σ_2, and σ_3, correspond to the compressional, intermediate, and extensional deviatoric stress axes, respectively, while the R ratio is a quantity describing relative stress magnitudes. To allow a well-constrained 3-D determination of the stress tensor, fault planes with different orientation are required, even if the total displacement they record is very low (sometimes at the millimeter scale). For poorly distributed fault sets (indicated with asterisk) we used an approach developed by *Bellier and Zoback* [1995]. This approach utilizes a "fixed" inversion, i.e., one in which the principal stress axes are fixed to lie in horizontal and vertical planes (considered generally to be the case in the Earth's crust). It was proved to be of good reliability, except for what concerns the R ratio. Site names are composed of a letter indicating the fault near which data were measured, and a number increasing northward (Figure 6). They are classified in relation to different stress regimes. Note that when a site shows two well-defined stress regimes we put them into two families of stress regimes. Column lithology can indicate the formations that record the data: undetermined bedrock (BR), Flysch (Fy), Gushi marls (Gu), Kheku sandstones (Kh), Pliocene Palami conglomerate (Pal), Pliocene Plc conglomerate (Plc), Quaternary undetermined (Q), Qt_{1a} or Qt_2. "Fisher" indicates the average stress obtained by computing stress axes using Fisher statistics on individual axes σ_1 σ_2 and/or σ_3 [*Fisher*, 1953]. MFP is the inversion of only the main fault planes, and PPF is an inversion of data on planes characteristic of the major faults, i.e., on data on planes parallel (same direction and plunge) to the major fault plane.

etc.) providing evidence of the present-day activity of this zone.

4. Fault Geometry of the Zagros-Makran Transfer Zone

[16] In order to examine potential partitioning of the deformation across the study area, we conducted a detailed mapping of the surface fault traces (Figure 5). This mapping was compiled by investigation of detailed geomorphologic fault characteristics on the basis of aerial photographs, satellite images, and fieldwork. We compiled a large-scale map of the fault systems which provides evidence for fault segmentation by identifying discontinuities such as step overs, relays, and bends. The region is characterized by two major fault systems which account for the major active deformation. They are separated by the broad Qal'e Manujan depression. These two fault systems will hereafter be referred to as the Zendan-Minab fault system to the west and the Sabzevaran-Jiroft fault system to the east.

4.1. Zendan-Minab Fault System

[17] The Zendan-Minab fault system runs along a NNW trending fold-and-thrust belt, 20 km wide and 250 km long, stretching from the Zagros (Main Zagros Thrust) in the north to the Oman Gulf coast to the south. It is oblique to the regional convergence and it is characterized by strike-slip, oblique reverse and thrust faulting as well as fault propagation folds and comprises three major fault zones which are, from west to east, the Minab, Zendan, and Palami fault zones (Figures 5 and 6).

[18] The Minab fault zone is conspicuous along about 50 km and trends parallel to the coast of the Hormoz Strait with a N160°E strike (Figure 5). It consists of a discontinuous and unlinear segment succession of east dipping thrust faults that affect the upper Cenozoic strata and the Quaternary deposits. North of Minab, the Minab fault allows the late Neogene sandstones and the lower Miocene Gushi marls to overthrust the middle Pleistocene upper pediment (Figures 4 and 7). This fault is intimately associated with a fold (the Minab fold) which runs parallel to the Zendan fault. Indeed, this fault largely marks the flank of the fold in its northern part. To the south, the fault obliquely crosscuts the fold near Minab. North of the fold, the thrust splits into two distinct segments. The western segment corresponds to an east dipping reverse fault affecting the upper Pleistocene fans at the front of the fold-and-thrust belt. The eastern segment is a NE dipping thrust that obliquely crosscuts the Minab fold. At its northernmost extremity, this thrust is sealed by the middle Pleistocene upper pediment surface (Qt_1, see age given by *Regard* [2003]).

[19] The NNW trending, east dipping, Zendan fault represents the main lithological boundary between the Zagros and the Makran. It is a roughly 250-km-long oblique reverse-lateral fault going from the Main Zagros Thrust (MZT), to the north, to the Gulf of Oman, to the south (Figures 2 and 5) [*Byrne et al.*, 1992; *McCall*, 1997]. The Zendan fault is highly segmented into segments of, on average, about 20 km in length (maximum length 35 km). Along the northernmost 50 km, the Zendan fault is arranged in en echelon segments (Figure 5). In the central part of the fault zone, it is characterized by relatively continuous traces locally marked by a west facing scarp within the Quaternary deposits.

[20] The Palami fault is an oblique reverse-lateral slip fault that tends parallel to the Zendan one. To the north, near the MZT (Main Zagros Thrust), it is not conspicuous. Near Minab, it is located 5 km east of the Zendan fault while to the south, it is 20 km away from the Zendan fault (Figure 5). It is less segmented than the Zendan fault with mean segment length of about 25 km and a maximum length of 41 km. The Palami fault trace is continuously underlined by east facing scarps affecting Quaternary fans. The fault splits

a

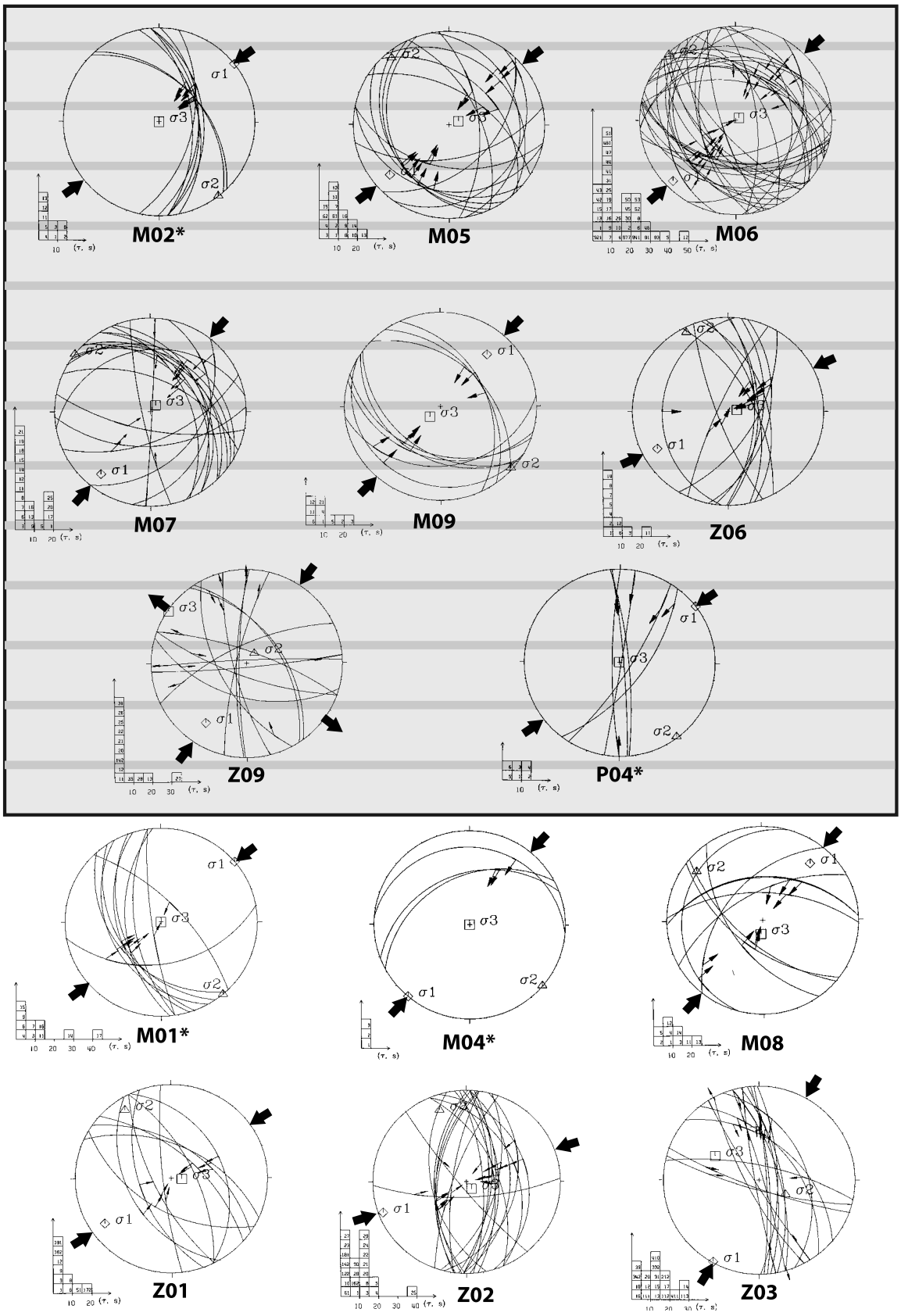

Figure 8

southward into two fault zones; one cuts through the coastal sediment around the Jask region, while the other is connected to the Makran prism deformation.

[21] To the north, the MZT is connected to the Zendan-Minab fault system through the 2700-m-high Kuh-e-Bandar Zagros fold. From north to south, the Zendan-Minab fault system is characterized by an across-strike width increase. It is formed by a single localized fault trace in the northern part, the Zendan fault, while the fault system is distributed in the southernmost zone and covers a 25-km-wide domain near Jask. In fact, the southern Zendan-Minab fault system termination bifurcates into two distinct faults zones. The first one is connected southeastward to the Makran prism thrusts through oblique structures with strikes ranged between N120°E and N150°E. This linkage between the Zendan-Minab fault system and the Makran thrusts at the western termination of the Makran prism could be responsible for the Makran's quite complicated relief (Figures 2 and 5). This first fault zone accounts for the major active deformation of the southern deformation of the Zendan-Minab fault system. The second fault zone is southward propagated within numerous fault branches arranged in a horsetail termination.

4.2. Jiroft-Sabzevaran Fault System

[22] The north striking Sabzevaran and Jiroft faults are characterized by linear fault traces bounding the eastern flank of two straight and narrow ophiolite horsts, of Paleozoic and Mesozoic ages, respectively [*McCall et al.*, 1985; *Kananian et al.*, 2001]. These east facing frontal fault zones consist of steep, fresh-looking scarps which mark the fault traces and are separated by a 15-km-wide undeformed zone. Both faults are highly segmented and affect the Quaternary fans and display evidence of geomorphic features like sag-ponds that testify to fault activity. The linearity of both faults suggests that they are nearly vertical (i.e., high angle west dipping fault) and accommodate predominantly strike-slip displacements (Figure 5). The western fault is the 60-km-long Sabzevaran fault, characterized by fault segments whose length ranges from 26 to 32 km. The eastern Jiroft fault, which marks the western boundary of the Jaz Murian depression, is about 75 km long and characterized by segments whose lengths range from 10 to 40 km. The northernmost parts of both the Jiroft and Sabzevaran fault zones are marked by distributed deformation over a broad area, arranged in horsetail terminations (Figure 5).

[23] The southern termination of the Sabzevaran fault is connected to the Jiroft fault by nearly NW trending segments, both faults being linked with the Makran thrusts at the southern edge of the Jaz Murian depression. However, minor deformation from the southern termination of the Sabzevaran fault seems to be transmitted southwestward as suggested by minor fault segments evinced by discontinuous geomorphic features across the Qal'e Manujan depression (Figure 5).

[24] A secondary 13-km-long fault segment, south of Kahnuj city, connects the Jiroft and Sabzevaran faults to the Kahnuj fault. It seems to run northward through major strike-slip faults to reach the active Nayband fault which marks the western boundary of the Lut block (Figure 1) [*Berberian*, 1981; *Walker and Jackson*, 2002].

4.3. Respective Roles of the Zendan-Minab and Jiroft-Sabzevaran Fault Systems

[25] Analyzing the distribution of the active faulting through the study area, i.e., the active geometry, of the Zendan-Minab and Jiroft-Sabzevaran fault systems, suggests they differ in terms of geodynamic significance. The Minab-Zendan-Palami fault system connects the Zagros deforming zone to the Makran and consequently transfers the active deformation from the continental wedge to the oceanic accretionary prism. Conversely, the Jiroft-Sabzevaran fault system is linking the Makran thrusts northward to other deforming zones (Alborz, Kopet Dagh or thrusts at the northern boundary of the central Iranian plateau) through the fault system constituted by the Nayband and Gowk faults (Figure 1), and thus it transfers part of the deformation related to the plate convergence toward the north.

5. Late Cenozoic Stress Regime and Fault Slip Vector Analyses

[26] The kinematics of a fault population is defined using the striations, corresponding to the slip vector, and measured on major fault planes as well as minor fault planes at several sites. The sites of fault slip measurements are shown in Figure 6 and the ages of the faulted formations from which the striae were measured are given in Table 2. We studied 33 sites located on the five main faults and covering an area of approximately 125×50 km^2. The methodology of fault kinematics studies to determine stress fields and to demonstrate temporal and spatial changes in the late Cenozoic stress states has been used in many active tectonic areas around the world over the past twenty [*Mercier et al.*, 1991; *Bellier and Zoback*, 1995; see references therein]. The inversion method used was initially proposed by *Carey* [1979]. Inversion results include the orientation (azimuth and plunge) of the principal stress axes of a stress tensor as well as a "stress ratio" $R = (\sigma_2 - \sigma_1)/(\sigma_3 - \sigma_1)$, a quantity describing relative stress magnitudes. Principal stress axes, σ_1, σ_2 and σ_3, correspond to the compressional, intermediate and extensional deviatoric stress axes, respectively. In particular, it provides information on the stress regime, i.e., compressional (reverse faulting stress state with σ_3

Figure 8. Lower-hemisphere stereoplots showing striation measurements together with results determined by *Carey*'s [1979] inversion method. See text and Table 2 for classification. Shaded zones represent measurements within Quaternary deposits. (a and b) Set indicating a N48°E trending horizontal σ_1 (compare Figure 15). (c) Set indicating a N83°E horizontal σ_1 (compare Figure 15).

b

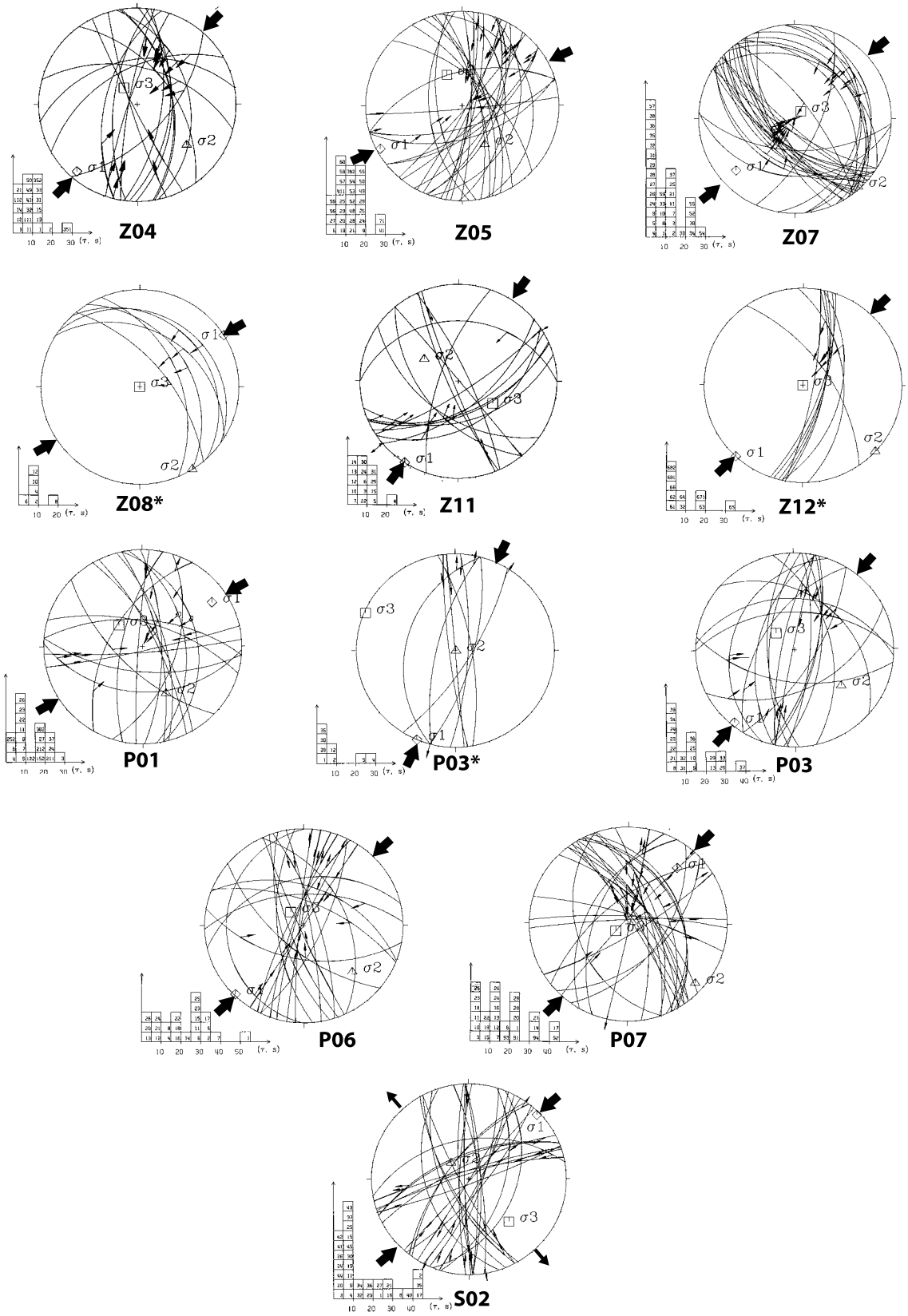

Figure 8. (continued)

c

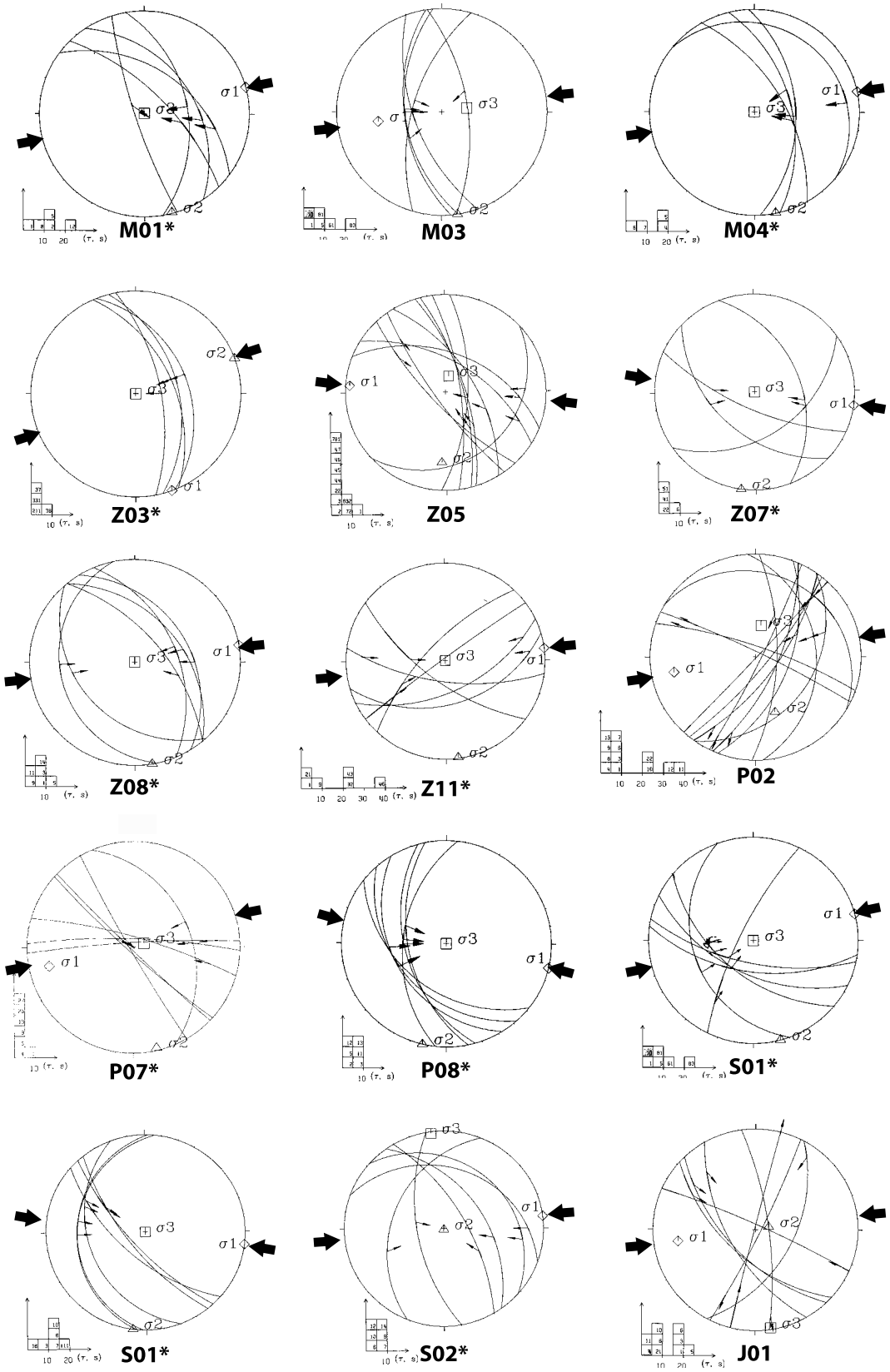

Figure 8. (continued)

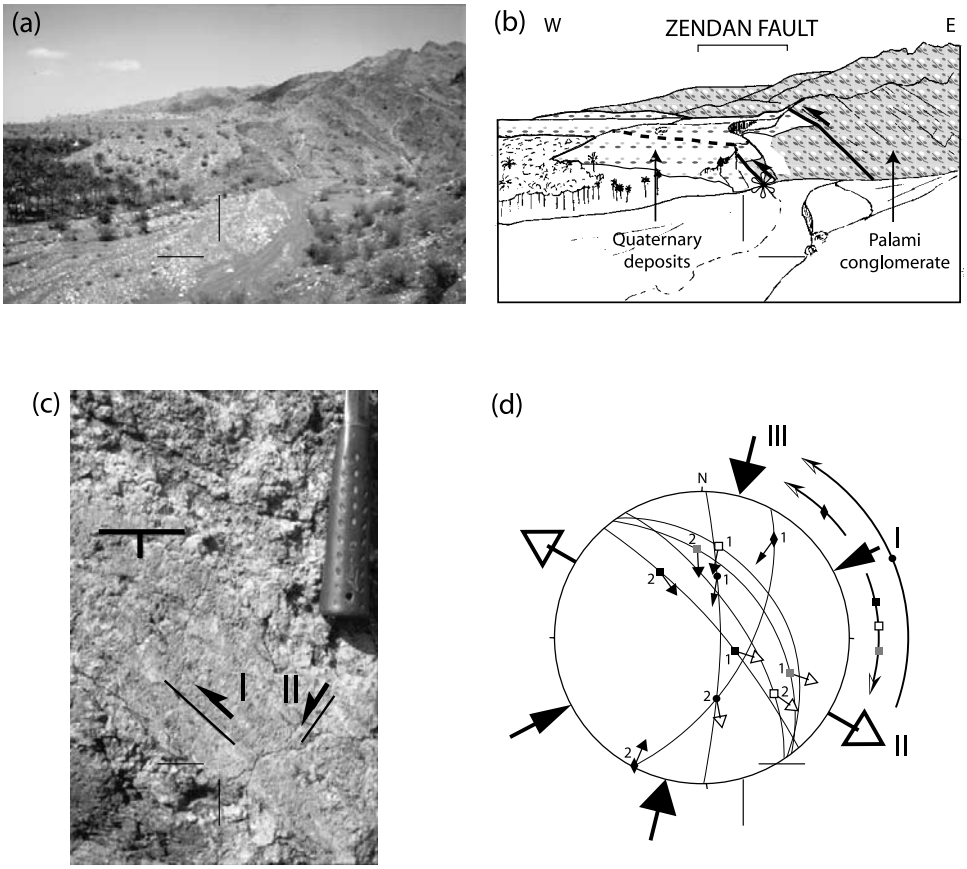

Figure 9. (a) North facing view of the Mir Hamar Ali oasis (Z05). (b) Interpretative drawing of Figure 9a. The Zendan fault is divided here into two or more faults. (c) Fault plane picture (located at the asterisk in Figure 9b) with two successive striae; I predates II. (d) Evidence of chronological succession of striations on lower-hemisphere stereoplot. Two striae with the same symbol are observed on the same plane with some evidence for relative chronology (1 is the older; 2 is the younger). Squares are striations reflecting the succession from the N62°E compressional stress regime (I) to the N120°E extensional regime (II). Circles show the succession from II to III (N15°E compressional stress regime). Diamonds show the transition from I to III.

vertical), strike-slip stress state (with σ_2 vertical), or transpressional (σ_2 or σ_3 vertical and σ_2 close to σ_3 in magnitude).

[27] The aim of this paper is to characterize the Quaternary to present-day stress in the Zagros-Makran transfer zone. Unfortunately, it is generally difficult to date the striations more precisely than by simply recording that they are younger than the rocks cut by the faults. In this study, we included results of measurements in flysch (sandstone layers), Gushi marls, Kheku sandstones, and Minab conglomerates as well as in recent alluvial and colluvial deposits. Often, more than one set of striae is present on a fault plane at the same measurement locality. However, distinct families of striations can be separated thanks to field observations (see below). Indeed, at some localities (as described in the following), reverse strike-slip striations caused by an E-W compression are crosscut by strike-slip striations resulting from a NE trending σ_1 compressional stress regime. These two contrasting sets of striae are observed along major fault planes or adjacent faults affecting rocks ranging in age from lower Miocene (Gushi marls) to Plio-Pleistocene (conglomerates). The discrimination of striae belonging to both sets is conducted by careful numerical check (by checking between the incompatible striae) and geological argumentation. The latter must be carried out on the basis of combined considerations of age of the faulted formation and relative chronology of the striations (crosscutting relationships), as well as their relation to regional tectonic events.

5.1. Fault Kinematics

[28] We have investigated the major Minab, Zendan, Palami, Jiroft, and Sabzevaran faults and the secondary Kahnuj fault (compare Figure 6). Their superficial trace usually consists of discontinuously steep, fresh-looking scarp at the foot of relieves. The Zendan, Minab and secondary Kahnuj faults are located west of the relief and are west facing (east dipping fault planes), while the others are east facing frontal faults associated with west dipping

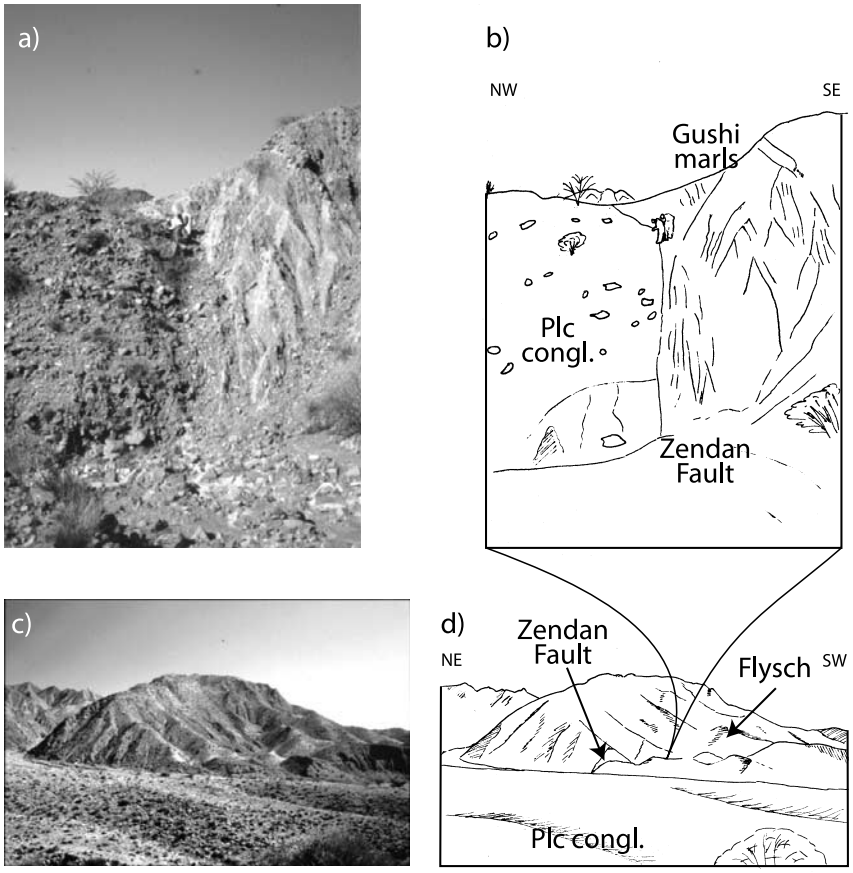

Figure 10. (a) Northeast facing view of the faulted contact between the Gushi marls and the Plc conglomerate at site Z08. The fault is the Zendan fault. (b) Sketch of Zendan fault. (c and d) General view of site Z08 and its interpretation showing the Zendan fault separating the Gushi marls and flysch from Plc conglomerates.

faults. None of the faults permits evaluation of the cumulate offsets on the major structures, but local recent offsets have been measured for slip rate determination [*Regard*, 2003].

5.1.1. Significant Sites of the Minab-Zendan Fault System

[29] The first site (M04) is located along the Minab fault, in the vicinity of the village of Demchehr, 13 km north of Minab, on the road to Bandar Abbas (Figure 6). At this site, the Minab fault trace corresponds to the thrust ramp associated with the westward verging Minab anticline. The Kheku sandstones, belonging to the Minab fold, overthrust the Quaternary primitive pediment (Qt_1, Figure 7). Slip measurements at site M04, located on the northern flank of the fans (27.28°N, 57.03°E) show two contrasting subsets on a north trending east dipping fault plane affecting the Kheku sandstones. The first population is mainly reverse, associated with dip-slip striae. The second is represented by oblique reverse-right-lateral slip vectors. These two subsets represent two successive stress regimes: The first corresponds to a purely compressional stress regime with a N78°E trending σ_1 and the second corresponds to a transpressional stress regime characterized by a N40°E trending σ_1 (Figures 7 and 8a–8c and Table 2).

[30] A second significant site is located along the Zendan fault, 16 km ESE from Minab city (30 km by the road), at Mir Hamar Ali oasis (site Z05, 27.09°N, 57.23°E; compare Figure 6). This site is situated at the foot of the Palami range. It is part of a former intramontane lower Pliocene basin that has been filled by the Palami conglomerate and then uplifted to its present-day position. Here the Zendan fault crosscuts a Quaternary alluvial formation contemporaneous with the primitive pediments [*McCall et al.*, 1985]. This formation is overthrusted by the Palami conglomerate (Figure 9). The site has some meter-scale fault planes parallel to the Zendan fault. Striations have been measured on these fault planes as well as on other minor planes, mainly in the Palami conglomerate. The 39 measured striae enable the discrimination of two successive compressional stress regimes: The first is characterized by a N94°E trending σ_1 and the second is characterized by a N62°E trending σ_1 (Figures 8a–8c and 9 and Table 2). Other minor

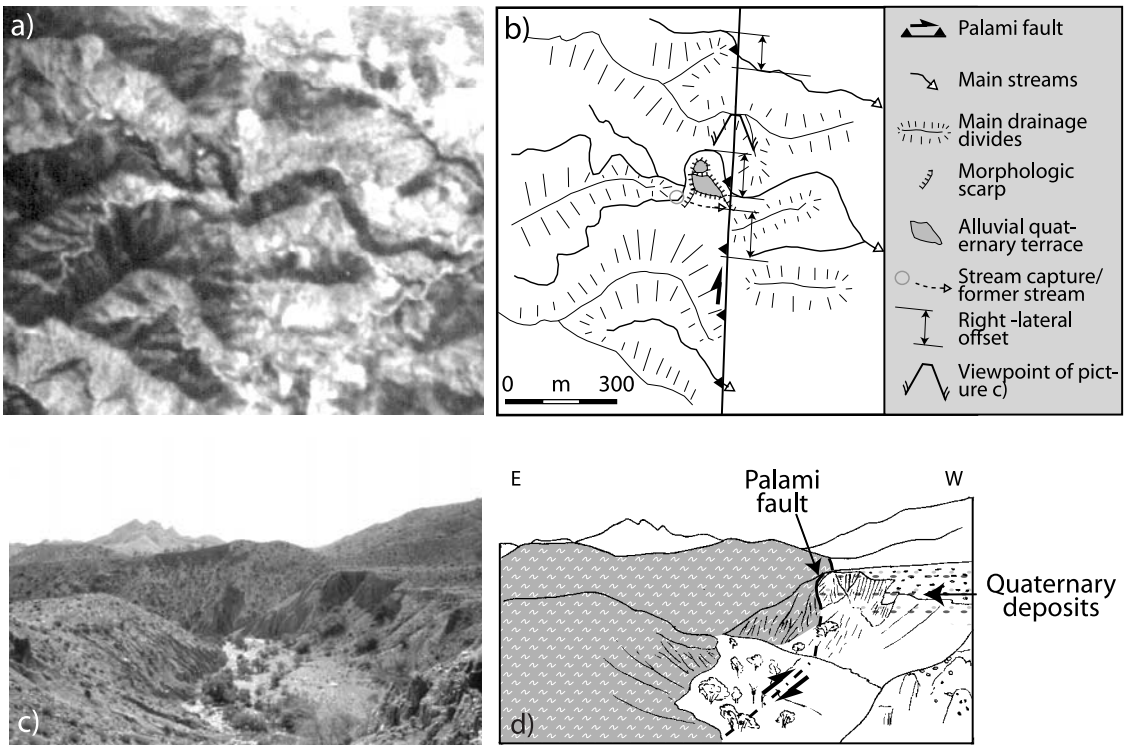

Figure 11. (a and b) Aerial photograph of location P04 and its interpretative sketch, top to the north. (c and d) South facing view of Palami fault and interpretative sketch.

and late normal striae overprint the previous ones. They have been interpreted as the results of recent gravitational effects.

[31] The site Z08 is also located near the Zendan fault, further north (30 km from Minab), 2 km south of the Bandar Abbas-Kahnuj road (27.42°N, 57.01°E; compare Figure 6). It is located between the Zendan mountain to the east and a valley filled by Pliocene Plc conglomerate, which separates the Minab fold from the Zendan mountain, to the west. On both field and aerial photographs, at Z08 the Zendan fault trace corresponds to the contact between the Gushi marls and Pliocene conglomerates (Plc, Figure 10). The fault is steep and has a reverse component that allows the marls to overthrust the conglomerate (Figure 10). Measurements on Plc pebble faces are related to two distinct stress states. They record reverse-faulting stress regimes, consistent with N58°E trending and 81°E trending compressional axes (Figures 8a–8c and Table 2).

[32] The first selected site of interest along the Palami fault is located SE of the Palami mountain (site P04, 27.08°N, 57.28°E; compare Figure 6). The eastern boundary of the Palami conglomerate is marked by a reverse fault, where the Palami conglomerate is topographically higher than the surrounding formations which form the Jaghin plain. At this location, stream offsets also indicate a dextral component of fault motion (Figure 11). The fault separates a Quaternary alluvial terrace from flysch. The fault plane is very steep (azimuth N5°E, dip 78°E; Figure 11) and striation measurements on pebbles from the terrace indicate a dextral strike-slip motion for the fault with a slight reverse component (pitch of 10°). Data inversion reveals a transpressional regime with a N52°E trending σ_1 stress axis (Figures 8a–8b and Table 2).

[33] Site P07 is located east of the Palami mountain near the Dast Kerd village (27.15°N, 57.26°E; Figure 6). The Palami fault corresponds there with an east facing 8-m-high geomorphic scarp (Figure 12) affecting a Quaternary terrace and carrying dextral offsets of streams (50–70 m). This scarp marks the frontal fault between the Palami mountain, constituted by Palami conglomerate, to the west, and the Jaghin plain, to the east, the fault trace trending N165°E. Striae measured in the upper Pliocene Plc conglomerate indicate a compressional stress with a N42°E trending σ_1 (Figures 8a–8b and Table 2). Another scarp, trending N135°E, cuts the deposits within the plain, 6 km northeast of Dast Kerd (Figures 12c and 12d). Site P08 (27.15°N, 57.28°E) is located on this scarp and displays evidence for a compressional regime associated with a N103°E trending σ_1 axis (six data; Figure 8c and Table 2).

5.1.2. Significant Sites of the Jiroft-Sabzevaran Fault System

[34] The Sabzevaran fault exhibits a fresh N-S scarp over 30 km along the road to Bandar Abbas, south of Kahnuj. It represents the boundary between the 1500 m elevated Gireh mountain to the west and the 600 m elevated Zamin Band-Bargah valley to the east (Figure 6). Its straight trace suggests a dominant strike-slip component for the present-day faulting. However, strike-slip and reverse faults postdate extensional penetrative deformation testified by normal-faulting striae and lineations on east dipping folia-

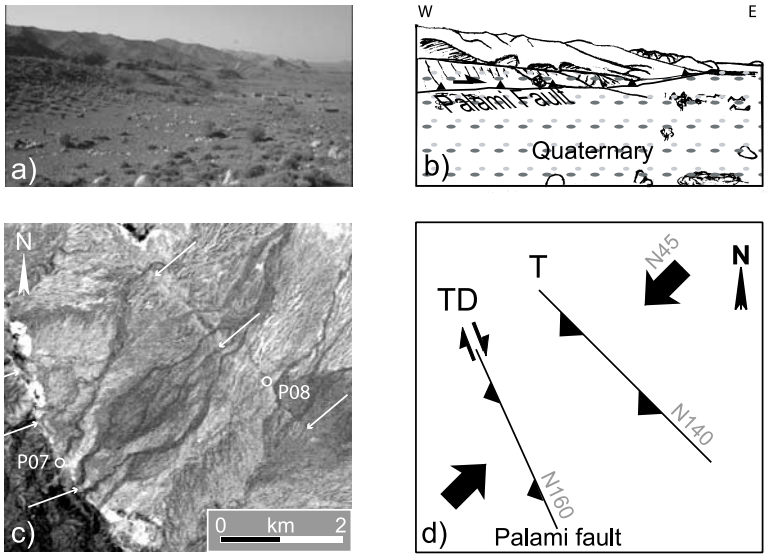

Figure 12. (a) North facing view of Palami fault at site P07 (Dast Kerd). (b) Interpretative drawing. (c) SPOT satellite image of the P07 and P08 locations. Fault traces are highlighted by white arrows. (d) sketch showing the relation between fault motion and azimuth and convergence direction. The fault at P08 has a N140°E azimuth, perpendicular to the convergence motion, and is a pure thrust (T). The Palami fault at Dast Kerd (P07) is oblique to the convergence motion. Its motion is reverse with dextral component (TD).

tion planes. This deformation could be responsible for the previous ophiolite ridge uplift, the relief probably being partly inherited.

[35] Site S02 is located on the trace of the Sabzevaran fault, at 27.79°N, 57.66°E, 18.5 km SSW from Kahnuj (Figures 6 and 13). A weathered Quaternary fan surface, of the same age as the Qt_{1a} pediment is dissected and partly covered by younger deposits. The oldest fan surface is 4.5 m vertically offset by the fault and some streams have been right-laterally offset by about 80 m. Striae are only observed and have only been measured in the basement. 6 of them indicate a N83°E trending σ_1 compressional regime while the other 29 allow the calculation of a N46°E trending σ_1 strike-slip stress regime (Figures 8a–8c). The latter is consistent with a dextral strike-slip movement on the major fault. Even if vertical fracture cleavage attests to recent strike-slip brittle deformation within the bedrock, none of the strike-slip fault planes have been observed to affect the Quaternary deposits.

[36] The Jiroft fault represents the boundary between a mountainous zone, to the west (Kuh-e-Khema, 1426 m), and the Jaz Murian depression, to the east. To the south it splits into several bifurcating segments connecting in a SE then east trending direction within the northern termination of the Makran range. Only one site has been analyzed along this fault (J01, 27.60°N, 57.80°E). It is located 40 km SSE of Kahnuj (Figure 6), on a fan surface made of meter-scale coarse materials. The fault trace cartographically bends eastward crossing the fan envelope, indicating a steep western dip for this fault (Figure 14). Inversion of the striae set in the basement yields a strike-slip stress regime characterized by a N80°E trending σ_1 axis (Figure 8b).

5.2. Regionally Significant Faulting Stress Regimes

[37] The two families measured at several sites suggest a change in the compressions responsible for successive faulting with an apparent rotation of the σ_1 direction which trends N83 ± 6°E then N47 ± 5°E (Figures 15 and 8a–8c and Table 2). Kinematics from the youngest striae agree with the fault slips from the striation affecting the Quaternary formations.

[38] Two other families of striae are less obviously observed. The first shows a north trending horizontal σ1 state of stress and affects Quaternary formations. The other is represented by normal faulting; the deduced extensional direction is not homogeneous. Both these stress states are only locally documented and their significance and relationship with the regionally consistent stress regime are not understood. We attribute them to local effects and refrain from further discussion.

[39] In an attempt to constrain the parameters of the stress regimes on a regional scale, we computed mean stress axes (with their 95% confidence cones) using McFadden's method, which gives Fisher statistics, computed by the PMSTAT software [*Enkin*, 1995]. This statistical analysis was carried out independently for each subset of individual site stress axes (e.g., subsets presented in Figures 8a–8c).

5.2.1. East Trending σ_1 Reverse Faulting Stress Regime

[40] Evidence for the east trending σ_1 reverse faulting stress regime is recorded throughout the Zagros-Makran

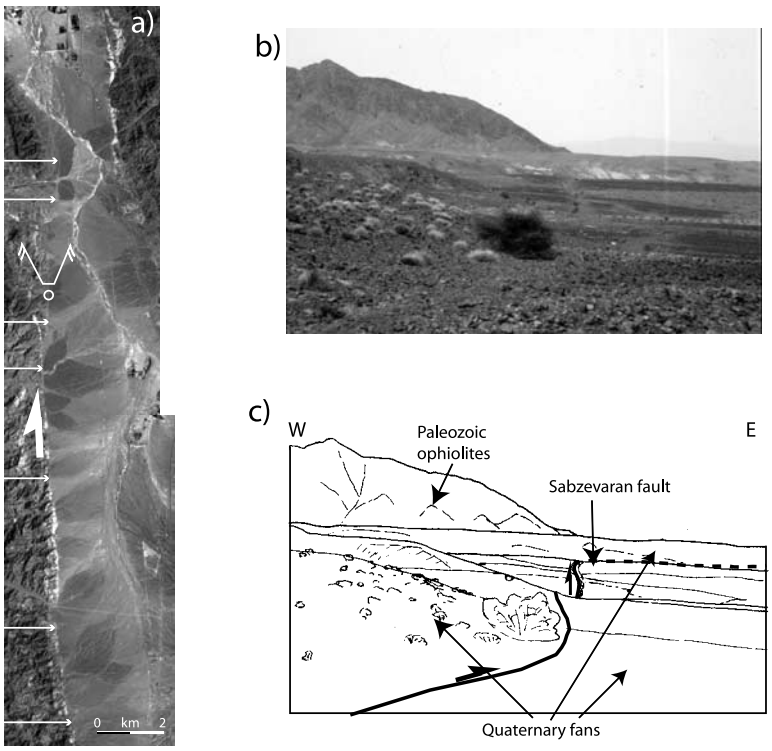

Figure 13. (a) SPOT satellite image of Sabzevaran fault. White arrows highlight its trace. Open circle is the location of site S02 with the direction of photograph in Figure 13b. (b and c) North facing view of Sabzevaran fault at site S02 and interpretative sketch.

transition zone by slip on faults which affect Pliocene conglomerates as well as Tertiary shallow marine deposits and Oligocene-Miocene flysch, as previously reported by *Kadjar et al.* [1976, 1978]. The results of data inversions are drawn in Figure 8c. All stress deviators indicate an east trending σ_1 axis, comprised between N70°E and N103°E, with a relatively well-constrained N83°E mean direction (5.9° 95% confidence angle α95; Table 1 and Figures 8c and 15). This regional stress regime is characterized by a mean N83 ± 6°E compressional direction, plunging 5° to the west, the vertical σ_3 axis favoring thrusting deformation. Since this stress state is both overprinted by the NE-SW compressional stress regime (see following), and recorded only by pre-Pleistocene formations, we assume it is representative of a pre-Pleistocene stress state.

5.2.2. NE Trending σ_1 Transpressional Stress Regime

[41] The NE trending σ_1 transpressional stress regime is widely observed throughout the entire study area (Figures 8a–8c). It has been observed in Quaternary deposits, as well as in older rocks (Figures 8a–8b), as already noted by *Kadjar et al.* [1976, 1978]. Thus it seems younger than the east trending σ_1 stress regime, which is only recorded in pre-Quaternary formations. The mean σ_1 axis direction is well constrained in a N48°E horizontal direction (1° dip), as indicated by his low, 5° confidence angle (α95). For this stress regime the σ_2 and σ_3 axis directions are not well constrained, i.e., contained within a plane perpendicular to the σ_1 mean axis (Figure 15; this is due to the fact that σ_2 and σ_3 values are very close). Additional analysis has been conducted by reporting the *R* value distribution on a histogram (Figure 15). It shows that *R* values are ranged from 0.3 to 1 with a maximum frequency near 0.8, suggesting a transpressional stress

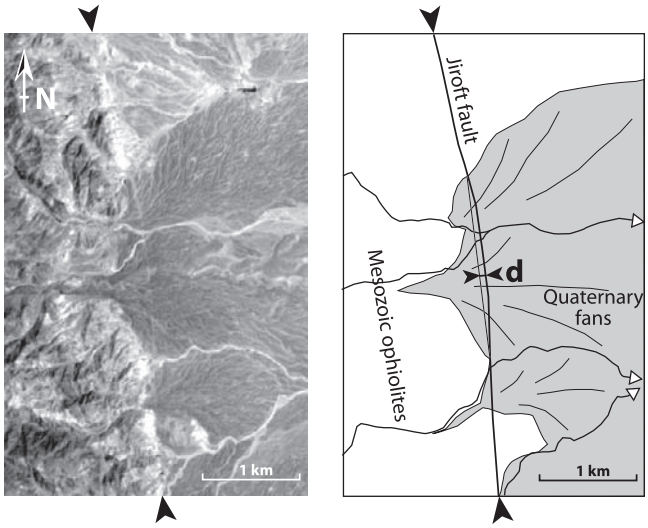

Figure 14. SPOT satellite image of site J01 and interpretative sketch (alluvial fans are shaded). Solid arrows show the Jiroft fault trace and "d" represents its deviation through alluvial fans, indicating the fault plane dips to the west.

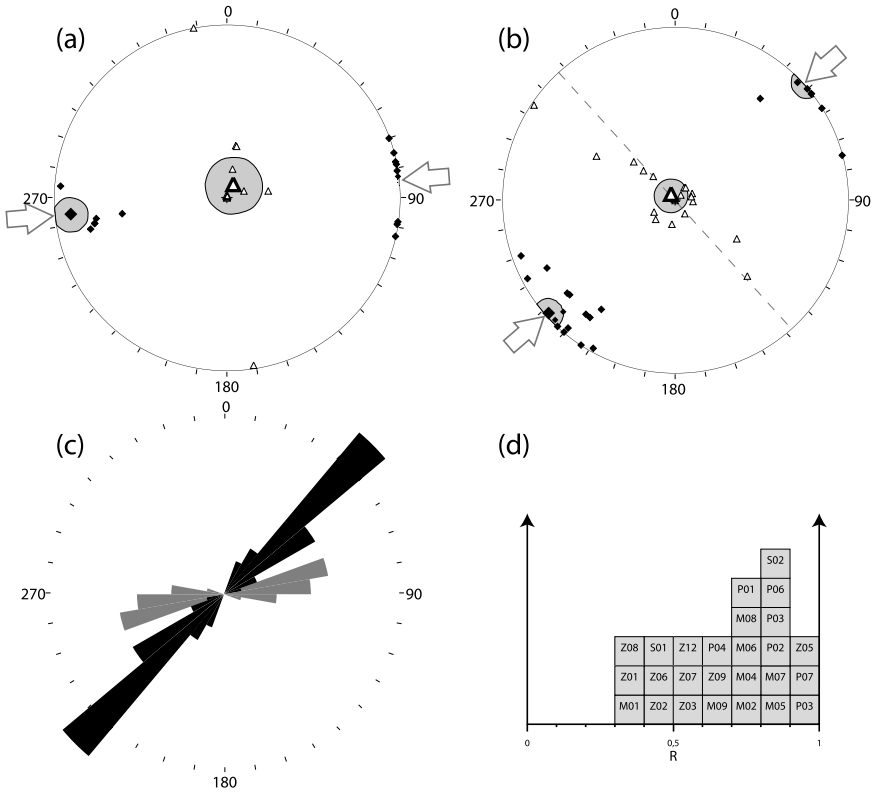

Figure 15. Statistics on inversion results. (a and b) Fisher statistics for stress regime up to Pliocene and Pliocene-Quaternary, respectively. Small diamonds and small triangles are σ_1 and σ_3 directions of inversions of Figures 8a–8c, respectively. Big symbols represent the statistic means of the directions represented by small symbols. Shaded area is the 95 per cent confidence zone (Table 2). Statistic mean of sites of Figure 8c is shown in Figure 15a. Arrows indicate that mean direction is compressional in a N83°E direction (5.9° 95% confidence angle α95). Statistic mean of sites of Figures 8a and 8b is shown in Figure 15b. Arrows indicate that mean direction is compressional in a N47°E direction (4.8° 95% confidence angle). The σ_3 mean direction is not well constrained; σ_3 directions are distributed around a plane perpendicular to the mean σ_1 direction (dashed line). (c) Rose diagram for the σ_1 frequency for 10° intervals. Solid and shaded parts represent measurements corresponding to young, Pliocene-Quaternary, or old, Pre-Pleistocene stress states, respectively. Note that the two sets are separated by less filled directions. (d) Histogram of the *R* values of the inversions of Figure 8c. In the squares are indicated the sites' names.

regime. This means that the σ_{hmin} axis is close in magnitude to σ_v, indicating a regional reverse-slip regime close to the transition to a strike-slip faulting one. This statistically significant regional stress regime can be compared to other regionally significant stress states calculated by striae inversions. Two inversions have been conducted. The first results from the computation of the major fault planes at each site (MFP; Table 2) and the second from the computation of the striations on planes parallel to the regional faults (PPF; Table 2). MFP is the result of the computation of 20 data with N44°E trending σ_1 and N135°E trending σ_2 axes, both axes being horizontal. The stress ratio *R* is 0.65, indicating that the deformation style is thrust faulting ($1 \gg R > 0.5; \sigma_1 \gg \sigma_2 > 0$). PPF is significantly consistent with the previous results with horizontal N49°E trending σ_1 and N139°E trending σ_2 axes. However, its deformation mode is close to a transitional one between thrust and strike-slip faulting, as indicated by the high *R* value ($R = 0.88$) and confirms the regionally significant transpressional stress regime.

[42] Several fault segments exhibit right-lateral offsets of geomorphic features; i.e., streams, late Quaternary alluvial fans, shutter ridges, etc., while prominent escarpment locally marked by a several-meters-high scarp within a Quaternary fan envelope indicates that a reverse-slip component characterizes the present-day faulting. These geomorphic characteristics indicate that both combined strike-slip and reverse-slip faulting currently occur through the study region. This geomorphic observation also implies a transpressional tectonic regime that has been confirmed by the GPS measurements [*Bayer et al.*, 2002]. Indeed, recent GPS data suggests a present-day transtensional regime in combination with NE trending shortening. Similarly, the analysis of the slip vector measured on the major fault planes affecting recent deposits confirms this

tectonic regime (see section on fault kinematics). The only available focal mechanism is consistent with the recent transpressive stress regime (see before).

[43] In detail, observations indicate the same stress regime for each fault. This implies that the deformation is not partitioned (i.e., onto parallel pure dip-slip and pure strike-slip faults) over the area. The kinematics of each fault is only dependent on its orientation with respect to the stress tensor, as shown in the sketch map of the Figure 12d. Actually, the displacement distribution on the faults hardly depends on fault orientations: (1) North trending faults, i.e., very oblique to the main compression (σ_1), are strike-slip, (2) NNW trending faults, less oblique to σ_1, have dextral-reverse oblique slip, and (3) NW trending faults, nearly normal to σ_1 are characterized by reverse dip slip.

[44] In conclusion, the youngest slip recorded by brittle deformation is very homogenous throughout the transfer zone, excluding the possibility of partitioning. It is characterized by a roughly N45°E main compressional direction, oblique with respect to the global direction of the Arabia-Eurasia convergence (Figure 1 and Table 1). The associated deformation is transpressional, with $\sigma_1 \gg \sigma_2 > \sigma_3$ and σ_3 vertical, and the regionally significant stress state is close to transition between reverse and strike-slip regime.

6. Discussion

[45] The present study provides evidence for a wide zone of fault deformation accommodating the oblique convergence of the Arabian-Eurasian plates and the relative motion of the Zagros and Makran wedges. This domain is made up of five major fault zones: the Minab, Zendan, Palami, Sabzevaran and Jiroft fault zones and the minor Kahnuj fault. The principal Zendan-Minab fault system of parallel faults trending N160°E and comprising the Zendan, Palami and Minab faults, links the Main Zagros Thrust to the Makran's active thrusts. Deformation does not seem to affect the shoreline and join the offshore frontal Makran thrust northeast of the study area, the Sabzevaran-Jiroft fault zone corresponds to north trending faults which are related to the Zagros-Makran transition, since it links inner Iran (Nayband fault) with the northwestern end of the Makran prism and the Zendan fault (Figures 1 and 2).

[46] Until recently, the regional deformation in the Zagros-Makran transition zone had not been accommodated only by faulting within the transfer zone. Folded upper Pliocene sediments partly overlying the Minab fold indicate a former phase of intense folding. Presently folds trend N160°E, i.e., parallel to the main faults and are arranged in right-lateral en echelon. For more recent episodes, the youngest striae indicate a Quaternary to present-day dominantly transpressional stress regime which induces both strike-slip and reverse faulting affecting Tertiary bedrock up to Recent formations and producing new faults or reactivating older ones. However, major (at the regional fault plane scale) and minor (at the slickenside scale) deformations provide evidence of a recent change in the faulting regime in this region, both regimes being characterized by reverse faulting (i.e., horizontal σ_1 and σ_2 axes). This change shown by striae chronologies and fault slip vector inversions, marks the transition between two successive pure reverse faulting and then oblique reverse-lateral faulting phases, the first with a nearly dip reverse component, the second with a right-lateral oblique component. It corresponds to a change from reverse faulting to a transpressional regime with, respectively, consistent east trending then NE trending σ_1 axes.

[47] Two alternative hypotheses can explain the apparent faulting regime change from E-W to NE-SW horizontal σ_1: either the shortening direction has really changed (i.e., as a result of regional/local rotation of stress axes), or the rocks in which they are measuring their shortening directions have rotated clockwise. The whole geological structure of the syntaxis around the Musandam peninsula suggests that rotations have taken place. However, paleomagnetic results, obtained after unfolding of two folds within the area, show that no significant rotation around vertical axes relative to Eurasia has occurred in these folds since Pliocene (see Figure 6 for the location of the folds) [*Delaunay et al.*, 2002].

[48] The presence of two sets of striae, the evidence of their chronological succession, as well as the low occurrence of intermediate orientation (i.e., 65° trending σ_1; Figure 15c), more probably indicate an abrupt stress change rather than a rotation of the study area. However, the occurrence of measurements with a σ_1 trending between 60° and 70° could be due to mechanical heterogeneities (spatial) resulting from local stress state heterogeneities (temporal variation) within a single regional stress regime. This phenomenon is currently observed within wide transcurrent shear zones, where local stress state can slightly change spatially with the change of the fault geometry [e.g., *Bellier et al.*, 1997].

[49] The penultimate stress regime, i.e., the east trending σ_1 reverse faulting stress state, is coeval with the right-lateral en echelon arrangement folding that affected Miocene up to the (lower) Pliocene. This suggests that the late Tertiary tectonic regime is partitioned within dip-slip reverse faulting and right-lateral en echelon folding consistent with an approximately NE trending regional compression; this partition allows the accommodation of both the lateral displacement due to the convergence obliquity and the shortening relative to the normal plate convergence (Figure 16). Some similar results showing the development of en echelon folds predating superficial thrusts have been found by *Wilcox et al.* [1973]; they could be related to thrusts developing at depth.

[50] Unfortunately, the geological control on the timing of the change is too poor to determine accurately the age of the change of the stress state. The age of the faulted formation suggests that the change occurred during sedimentation of the upper Pliocene (Plc) conglomerates. Even if poorly constrained, deposition of these conglomerates and the change in tectonic regime possibly occurred in late Pliocene times. This is contemporaneous with the major Pliocene geodynamic events which have been reported throughout the Iranian domain. Indeed, major change within the Iranian tectonic has been documented at about 3–5 Ma

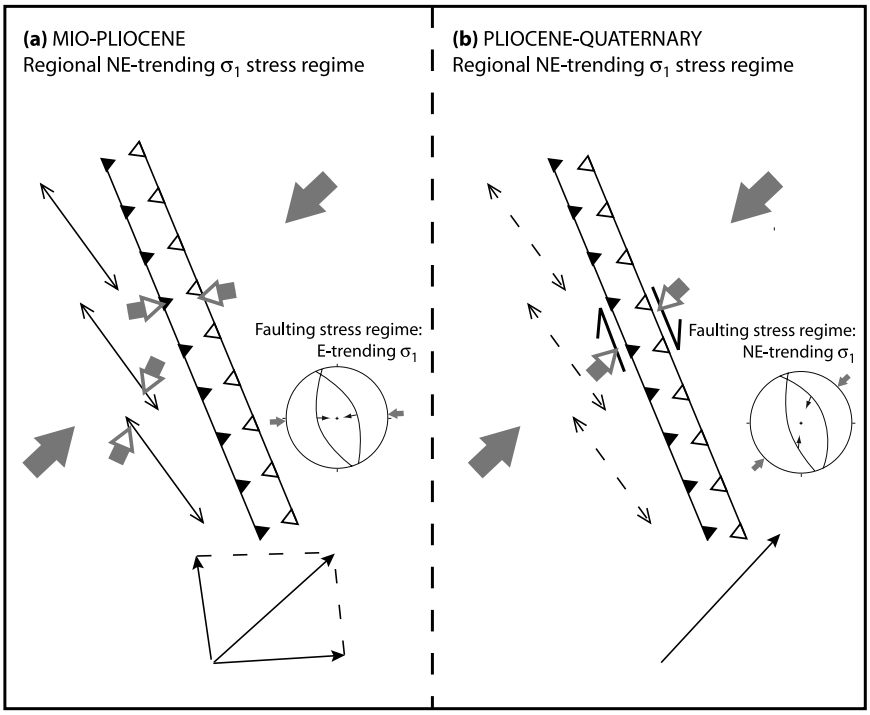

Figure 16. Schematic drawing for the different ways of accommodation of the N45°E trending convergence during the Mio-Pliocene and the Pliocene-Quaternary periods. Solid arrows indicate regional σ_1 direction; open arrows indicate σ_1 around folds and faults. Lower-hemisphere stereoplots indicate principal fault planes with the observed striae associated. (a) During the Mio-Pliocene, some partition occurs between folds, accommodating N-S convergence and faults accommodating E-W convergence. (b) During the Plio-Quaternary, there is just distribution of the deformation on parallel faults, each accommodating some NE-SW convergence.

[*Falcon*, 1974]. There are several possible explanations for this reorganization [*Allen et al.*, 2003b]. (1) Arabia accelerated from Africa at 4–5 Ma, as oceanic spreading began in the Red Sea [*Ghebreab*, 1998]. (2) At ~5 Ma, strain across the Caucasus decreased [*Zonenshain and Le Pichon*, 1986], and thus may have been taken up elsewhere, in Iran, for example. (3) Construction of the Turkish-Iranian Plateau took place in the upper Miocene, but ceased at about 5 Ma, possibly because it became easier to shorten and thicken the crust in peripheral areas of the collision zone than to continue uplifting the plateau [*Allen et al.*, 2003b]. We suspect that the change that occurred in the study area could be related with this regional reorganization, i.e., around 3–5 Ma.

[51] The transpressional character of the recent stress regime explains the compatibility between the observed reverse and strike-slip faulting. The trends of the horizontal stress axes for both old compressional and modern transpressional regimes obtained from the strike-slip striae are relatively consistent throughout the studied region, i.e., over distances of about 200 × 100 km. This remarkably homogeneous stress field is characterized by stress trends almost parallel throughout the study area (constant orientation). This indicates that the determined stress regime is regionally significant and supports the suggestion that regionally large-scale block rotation did not occur in the studied region during the Quaternary. Only small perturbations in the horizontal stress axes were observed locally (e.g., local normal faulting and north trending compression). They could result from small-scale block rotations within narrow zones of intense deformation in or adjacent to the fault zones. The homogeneity of the present-day stress-regime implies that there is no partitioning between the faults (Figure 16). Even if the faults have different motions, from pure dip slip to pure strike slip, it is only due to their orientation with respect to the far-field stress pattern, not to partitioning (Figure 12d).

[52] Even if there is no partitioning in the Zagros-Makran transfer zone, the stress state around the fault (~N45°E directed σ_1) does not correspond to the orientation of the plate convergence vector (~N10°E), but it agrees with the shortening axis given by GPS measurements [*Bayer et al.*, 2002].

[53] In this scheme, the two fault systems constituting the study area do not have the same significance. One (the Minab-Zendan-Palami Fault system) connects the Zagros and Makran wedges, whereas the second (the Jiroft-Sabzevaran) transmits some deformation from the Makran thrust further north. Thus the latter has a similar role to the Neh-Zahedan strike-slip fault zone, further to the east [*Freund*, 1970; *Tirrul et al.*, 1983; *Jackson et al.*, 1995; *Berberian et al.*, 2001; *Walker and Jackson*, 2002]; the importance of these zones has been stated by *Vernant et al.* [2004]. Consequently, the study area does not constitute the

entire transition zone between Zagros and Makran, this being almost 500 km wide. The width of this transition, as well as the greater coupling of the Makran near the study area, may indicate that the subducting plate under Makran and Zagros is continuous.

[54] The contemporaneous motion of the two N-S fault systems (Nayband-Gowk and Neh-Zahedan) may have influenced the tectonics of the western part of the Makran between them (Figures 1 and 3), and the east Iranian ranges may divide the Makran into two distinct parts [*Byrne et al.*, 1992]. The structures appear to be more oblique with respect to the convergence vector as they are closer to the Zendan-Minab fault system, explaining the obliquity of the thrusts we observed. This feature could be the result of a large-scale drag, as is observed around the well-developed Chaman fault which accommodates the different motion between eastern Makran and the Himalayas. If the Zagros fold-and-thrust belt continues its growth in the future, the Zendan-Minab fault system will become a transform fault like the Chaman.

7. Conclusion

[55] The Minab area, at the transition between the Zagros collisional wedge and the Makran accretionary wedge over a subduction zone, is deformed by structures that are highly oblique (N150°E to N0°E) to the convergence vector (N10°E). Detailed mapping and striae data inversion lead to the conclusion that the present-day deformation is distributed over two fault systems without any partitioning. The tectonic regime through the study area is homogeneously transpressional with a NE trending σ_1. This represents a recent setting, since during the Pliocene there seems to have been some partitioning between pure reverse faulting related to east trending shortening and right-lateral en echelon arranged folds.

[56] The faults form two major fault systems, the western one transferring the Zagros deformation to the Makran, while the eastern one is connecting the Makran to the Alborz and Kopet Dagh deforming system, to the north. Consequently, this second system allows the transmission of part of the compression related to the plate convergence toward the north of Iran. At a regional scale, the convergence between the Oman Gulf (Arabian plate) and Eurasia is accommodated by the Makran thrusts. Nevertheless, Arabian plate drift at the west is not completely accommodated by the Zagros continental prism deformation since north of the Makran, the north trending Nayband, Neh and Zahedan faults are laterally slipping rapidly (2 mm yr^{-1}, 12 mm yr^{-1}, and 2.5 mm yr^{-1}, respectively) [e.g., *Jackson et al.*, 1995; *Berberian et al.*, 2001; *Walker and Jackson*, 2002]. As a result, part of the plate convergence is transmitted northward through the Iranian bock by north striking major strike-slip faults up to the northernmost Iranian deformation domain. This confirms that the Zagros accommodates only a part of the plate convergence, and that there is compressional deformation accommodating the plate convergence within mountain belts to the north, like the Alborz (Figure 3) [*Jackson et al.*, 2002; *Vernant et al.*, 2004].

[57] **Acknowledgments.** This work is part of the cooperative research agreement between the INSU-CNRS (France) and the International Institute of Earthquake Engineering and Seismology (IIEES, Iran), supervised by D. Hatzfeld and M. G. Ashtyani. We thank IIEES for fieldwork assistance and M. Mokhtari for support and administrative assistance. Funding was provided by the Intérieur de la Terre program (IT, INSU-CNRS) and the IIEES within the above mentioned cooperative agreement. The preliminary reconnaissance fieldwork around the Minab area was done with J. Mercier, and we have benefited from the observations that he completed 20 years ago with J.-J. Dufaure, C. Thibault, and M. H. Kadjar. SPOT images were provided thanks to ISIS program support (CNES). Satellite image analyses and mapping were performed thanks to the STSI CEREGE facility. We thank D. Chardon, J. Martinod, and D. L. Bourlès for their revisions of an early version of the manuscript and D. Hatzfeld and R. Walker for helpful discussions, respectively, on the seismotectonic context and on the role of the Nayband, Neh, and Zahedan faults. We are grateful to J. Jackson, R. Westaway, M. Bonini, and an anonymous reviewer, and Associate Editor A. Pfiffner, who helped to improve an earlier version of this manuscript. We are indebted to Tom Rutledge and Annabel Whibley for English improvement of this manuscript.

References

Ala, M. A. (1974), Salt diapirism in southern Iran, *AAPG Bull.*, *58*, 1758–1770.

Alavi, M. (1994), Tectonics of the Zagros orogenic belt of Iran: New data and interpretations, *Tectonophysics*, *229*, 211–238.

Allen, M. B., M. R. Ghassemi, M. Shahrahi, and M. Qorashi (2003a), Accommodation of late Cenozoic oblique shortening in the Alborz range, northern Iran, *J. Struct. Geol.*, *25*, 659–672.

Allen, M. B., J. A. Jackson, S. J. Vincent, E. J.-P. Blanc, M. R. Ghassemi, C. Davies, M. D. Simmons, and A. Ismail-Zadeh (2003b), Plio-Quaternary reorganisation of the Arabia-Eurasia collision, paper presented at AAPG Annual Convention 2003, Am. Assoc. Pet. Geol., Salt Lake City, Utah.

Ambraseys, N. N., and C. P. Melville (1982), *A History of Persian Earthquakes*, 219 pp., Cambridge Univ. Press, New York.

Bayer, R., et al. (2002), Active deformation in Zagros-Makran transition zone inferred from GPS, tectonic and seismological measurements, *Eos Trans. AGU*, *83*(47), Fall Meet. Suppl., Abstract S62B-1188.

Bellier, O., and M. Sébrier (1995), Is the slip rate on the Great Sumatran fault accommodated by fore-arc stretching?, *Geophys. Res. Lett.*, *22*, 1969–1972.

Bellier, O., and M. L. Zoback (1995), Recent state of stress change in the Walker Lane zone, western Basin and Range province, United States, *Tectonics*, *14*, 564–593.

Bellier, O., S. Över, A. Poisson, and J. Andrieux (1997), Recent temporal change in the stress state and modern stress field along the North Anatolian Fault Zone (Turkey), *Geophys. J. Int.*, *131*, 61–86.

Berberian, M. (1981), Active Faulting and Tectonics of Iran, in *Zagros, Hindu Kush, Himalaya, Geodynamic evolution*, *Geodyn. Ser.*, vol. 3, edited by H. K. Gupta and F. M. Delany, pp. 33–69, AGU, Washington D. C.

Berberian, M. (1995), Master "blind" thrust faults hidden under Zagros folds: Active basement tectonics and surface morphotectonics, *Tectonophysics*, *241*, 193–224.

Berberian, M., J. A. Jackson, E. Fielding, B. E. Parsons, K. Priestley, M. Qorashi, M. Talebian, R. Walker, T. J. Wright, and C. Baker (2001), The 1998 March 14 Fandoqa earthquake (M_w 6.6) in Kerman province, Southeast Iran: Re-rupture of the 1981 Sireh earthquake fault, triggering of slip on adjacent thrusts and active tectonics of the Gowk fault zone, *Geophys. J. Int.*, *146*, 371–398.

Blanc, E. J.-P., M. B. Allen, S. Inger, and H. Hassani (2003), Structural styles in the Zagros Simple Folded Zone, Iran, *J. Geol. Soc. London*, *160*, 401–412.

Bonini, M., G. Corti, D. Sokoutis, G. Vannucci, P. Gasperini, and S. Cloetingh (2003), Insights from scaled analogue modelling into the seismotectonics of the Iranian region, *Tectonophysics*, *376*, 137–149.

Boulin, J. (1991), Structures in southwest Asia and evolution of the eastern Tethys, *Tectonophysics*, *196*, 211–268.

Byrne, D. E., L. R. Sykes, and D. M. Davis (1992), Great thrust earthquakes and aseismic slip along the plate boundary of the Makran subduction zone, *J. Geophys. Res.*, *97*, 449–478.

Carbon, D. (1996), Tectonique post-obduction des montagnes d'Oman dans le cadre de la convergence Arabie-Iran, Ph.D. thesis, 408 pp., Montpellier II, Montpellier, France.

Carey, E. (1979), Recherche des directions principales des contraintes associées au jeu d'une population de failles, *Rev. Geol. Dyn. Geogr. Phys.*, *21*, 57–66.

Colman-Sadd, S. P. (1978), Fold development in Zagros Simply Folded Belt, southwest Iran, *AAPG Bull.*, *62*, 984–1003.

Delaunay, S., B. Smith, and C. Aubourg (2002), Asymmetrical fold test in the case of overfolding: Two examples from the Makran accretionary prism (southern Iran), *Phys. Chem. Earth*, *27*, 1195–1203.

DeMets, C., R. G. Gordon, D. F. Argus, and S. Stein (1990), Current plate motions, *Geophys. J. Int.*, *101*, 425–478.

Dufaure, J.-J. (1984), Piémont et transversale: Le contact Makran-Zagros (Iran du Sud), in *Montagnes et Piémonts*: *Actes du Colloque de géomorphologie*, pp. 423–426, Rev. Geogr. des Pyrénées et du Sud-Ouest, Toulouse, France.

Dufaure, J. J., C. Thibault, M. H. Kadjar, and J. L. Mercier (1978), La zone de failles du Zendan (Iran du Sud-Est): I-Géomorphologie et Stratigraphie du Quaternaire, paper presented at Réunion Annuelle des Sciences de la Terre (6th RAST), Soc. Geol. de Fr., Orsay, France.

Dziewonski, A. M., T.-A. Chou, and J. H. Woodhouse (1981), Determination of earthquake source parameters from waveform data studies of global and regional seismicity, *J. Geophys. Res.*, *86*, 2825–2852.

Enkin, R. J. (1995), A computer program package for analysis and presentation of paleomagnetic data—PMSTAT, vol. 1995, Pac. Geosci., Cent., Geol. Surv. of Can., Sidney, B. C., Canada.

Falcon, N. L. (1974), Southern Iran: Zagros mountains, *Geol. Soc. Spec. Publ.*, *4*, 199–211.

Farhoudi, G. (1978), A comparison of Zagros geology to island arcs, *J. Geol.*, *86*, 323–334.

Faure-Muret, A., and G. Choubert (1971), Aperçu de l'évolution structurale de l'Iran, in *Tectonique de l'Afrique*, *Earth Sci. Ser.*, vol. 6, pp. 141–151, UNESCO, Paris.

Fisher, R. A. (1953), Dispersion on a sphere, *Proc. R. Soc. London, Ser. A*, *217*, 295–305.

Fitch, T. J. (1972), Plate convergence, transcurrent faults and internal deformation adjacent to southeast Asia and the western Pacific, *J. Geophys. Res.*, *77*, 4432–4460.

Freund, R. (1970), Rotation of strike-slip faults in Sistan, southeast Iran, *J. Geol.*, *78*, 188–200.

Fruehn, J., R. S. White, and T. A. Minshull (1997), Internal deformation and compaction of the Makran accretionary wedge, *Terra Nova*, *9*, 101–104.

Garzanti, E., S. Critelli, and R. V. Ingersoll (1996), Paleogeographic and paleotectonic evolution of the Himalayan Range as reflected by detrital modes of Tertiary sandstones and modern sands (Indus transect, India and Pakistan), *Geol. Soc. Am. Bull.*, *108*, 631–642.

Gaudemer, Y., P. Tapponnier, B. Meyer, G. Peltzer, G. Shunmin, C. Zhitai, D. Huagung, and I. Cifuentes (1995), Partitioning of crustal slip between linked, active faults in the eastern Qilian Shan, and evidence for a major seismic gap, the "Tianzhu Gap," on the western Haiyuan fault, Ganzu (China), *Geophys. J. Int.*, *120*, 599–645.

Ghebreab, W. (1998), Tectonics of the Red Sea region reassessed, *Earth Sci. Rev.*, *45*, 1–44.

Harms, J. C., H. N. Cappel, and D. C. Francis (1984), The Makran coast of Pakistan: Its stratigraphy and hydrocarbon potential, in *Marine Geology and Oceanography of Arabian Sea and Coastal Pakistan*, edited by B. U. Haq and J. D. Milliman, pp. 3–26, Van Nostrand Reinhold, New York.

Jackson, J., J. Haines, and W. Holt (1995), The accommodation of Arabia-Eurasia plate convergence in Iran, *J. Geophys. Res.*, *100*, 15,205–15,219.

Jackson, J. A., K. Priestley, M. Allen, and M. Berberian (2002), Active tectonics of the South Caspian Basin, *Geophys. J. Int.*, *148*, 241–245.

Jacob, K. H., and R. L. Quittmeyer (1979), The Makran region of Pakistan and Iran: Tranch-arc system with active plate subduction, in *Geodynamics of Pakistan*, edited by A. Farah and K. A. de Jong, pp. 305–317, Geol. Surv. of Pakistan, Quetta.

Kadjar, M. H., J. L. Mercier, and L.-E. Ricou (1976), Les mouvements Plio-Pléistocènes de l'accident du Zendan, faille transformante intra-continentale entre le Zagros et le Makran (Iran)?, paper presented at Réunion Annuelle des Sciences de la Terre (4th RAST), Soc. Geol. de Fr., Paris, France.

Kadjar, M. H., J. L. Mercier, J. J. Dufaure, and C. Thibault (1978), La zone de failles du Zendan (Iran du Sud-Est): II - Etats de contrainte successifs post-Miocène inférieur le long de la limite orientale, intracontinentale, de la plaque arabique, paper presented at Réunion Annuelle des Sciences de la Terre (6th RAST), Soc. Geol. de Fr., Orsay, France.

Kananian, A., T. Juteau, H. Bellon, A. Darvishzadeh, M. Sabzehi, H. Whitechurch, and L.-E. Ricou (2001), The ophiolite massif of Kahnuj (western Makran, southern Iran): New geological and geochronological data, *C. R. Acad. Sci. Paris*, *332*, 543–552.

Kopp, C., J. Fruehn, E. R. Flueh, C. Reichert, N. Kukowski, J. Bialas, and D. Klaeschen (2000), Structure of the Makran subduction zone from wide angle and reflection seismic data, *Tectonophysics*, *329*, 171–191.

Koyi, H. A., K. Hessami, and A. Teixell (2000), Epicenter distribution and magnitude of earthquakes in fold-thrust belts: Insights from sandbox models, *Geophys. Res. Lett.*, *27*, 273–276.

McCaffrey, R. (1992), Oblique plate convergence, slip vectors, and forearc deformation, *J. Geophys. Res.*, *97*, 8905–8915.

McCall, G. J. H. (1997), The geotectonic history of the Makran and adjacent areas of southern Iran, *J. Asian Sci.*, *15*, 517–531.

McCall, G. J. H., and R. G. W. Kidd (1982), The Makran, southeastern Iran: The anatomy of a convergent plate margin active from Cretaceous to present, in *Trench Forearc Geology*, edited by J. K. Legget, *Geol. Soc. Spec. Publ.*, *10*, 387–397.

McCall, G. J. H., et al., (1985), Minab quadrangle map 1:250,000 and explanatory text, 534 pp., Geol. Surv, of Iran, Tehran.

McClusky, S., et al. (2000), Global Positioning System constraints on plate kinematics and dynamics in the eastern Mediterranean and Caucasus, *J. Geophys. Res.*, *105*, 5695–5719.

McClusky, S. M., R. Reillinger, S. Mahmoud, D. Ben Sari, and A. Tealeb (2003), GPS constraints on Africa (Nubia) and Arabia plate motions, *Geophys. J. Int.*, *155*, 126–138.

Mercier, J.-L., E. Carey-Gailhardis, and M. Sébrier (1991), Paleostress determinations from fault kinematics: Application to the neotectonics of the Himalayas-Tibet and the central Andes, *Philos. Trans. R. Soc. London*, *337*, 41–52.

O'Brien, C. A. E. (1957), Salt diapirism in south Persia, *Geol. Mijnbouw*, *19*, 357–376.

Regard, V. (2003), Lateral and temporal evolution from subduction to collision: Insights from Iranian tectonics (Zagros-Makran) and physical modeling (in French and English), thèse de doctorat, 358 pp., Univ. Aix-Marseille III. (Available at http://tel.ccsd.cnrs.fr/documents/archives0/00/00/37/77/index_fr.html)

Richard, P., and P. Cobbold (1990), Experimental insights into partitioning of fault motions in continental convergent wrench zones, *Ann. Tectonicae*, *4*, 35–44.

Ricou, L. E., J. Braud, and J. H. Brunn (1977), Le Zagros, *Mem. Soc. Geol. Fr.*, *8*, 33–52.

Sella, G. F., T. H. Dixon, and A. Mao (2002), REVEL: A model for Recent plate velocities from space geodesy, *J. Geophys. Res.*, *107*(B4), 2081, doi:10.1029/2000JB000033.

Talebian, M., and J. Jackson (2002), Offset on the Main Recent fault of NW Iran and implications for the late Cenozoic tectonics of the Arabia-Eurasia collision zone, *Geophys. J. Int.*, *150*, 422–439.

Tatar, M., D. Hatzfeld, J. Martinod, A. Walpersdorf, M. Ghafori-Ashtiany, and J. Chery (2002), The present-day deformation of the central Zagros from GPS measurements, *Geophys. Res. Lett.*, *29*(19), 1927, doi:10.1029/2002GL015427.

Tirrul, R., I. R. Bell, R. J. Griffith, and V. E. Camp (1983), The Sistan suture zone of eastern Iran, *Geol. Soc. Am. Bull.*, *94*, 134–150.

Vernant, P., et al. (2004), Contemporary crustal deformation and plate kinematics in Middle East constrained by GPS measurements in Iran and northern Oman, *Geophys. J. Int.*, *157*, 381–398.

Walker, R., and J. Jackson (2002), Offset and evolution of the Gowk fault, SE Iran: A major intra-continental strike-slip system, *J. Struct. Geol.*, *24*, 1677–1698.

Ward, S. N., and G. Valensise (1996), Progressive growth of San Clemente Island, California, by blind thrust faulting: Implications for fault slip partitioning in the California Continental Borderland, *Geophys. J. Int.*, *126*, 712–734.

White, R. S. (1982), Deformation of the Makran accretionary sediment prism in the Gulf of Oman (northwest Indian Ocean), in *Trench-Forearc Geology: Sedimentation and Tectonics on Modern and Ancient Active Plate Margins*, edited by J. K. Leggett, *Geol. Soc. Spec. Publ.*, *10*, 69–84.

Wilcox, R. E., T. P. Harding, and D. R. Seely (1973), Basic wrench tectonics, *AAPG Bull*, *57*, 74–96.

Zhang, Peizhen, P. Molnar, and W. R. Downs (2001), Increased sedimentation rates and grain sizes 2–4 Myr ago due to the influence of climate change on erosion rates, *Nature*, *410*, 891–897.

Zonenshain, L. P., and X. Le Pichon (1986), Deep basins of the Black Sea and Caspian Sea as remnants of Mesozoic back-arc basins, *Tectonophysics*, *123*, 181–211.

M. R. Abbassi, K. Feghhi, E. Shabanian, and S. Soleymani, International Institute for Earthquake Engineering and Seismology (IIEES), 27 Sholeh Street, 8th Kohestan, Pasdaran, P. O. Box 19395, 3913, Tehran, I. R. Iran.

O. Bellier and V. Regard, CEREGE, Europôle Méditerranéen de l'Arbois, BP 80, F-13545 Aix en Provence Cedex 04, France. (regard@cerege.fr)

J. Mercier, 1 allée traversière, F-94260 Fresnes, France.

J.-C. Thomas, Schönstr., 52b, D-81543, Münich, Germany.

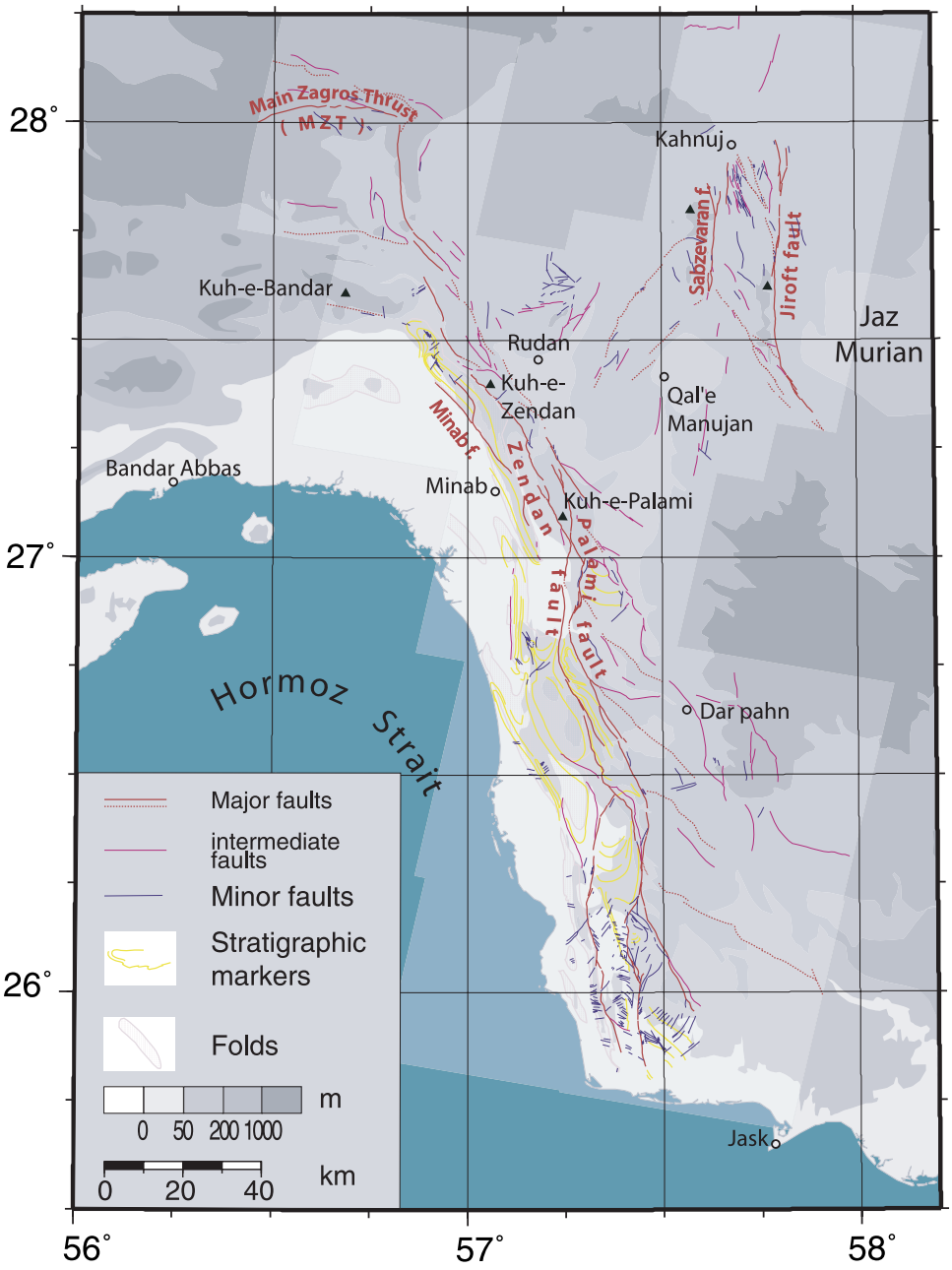

Figure 5. Structural and tectonic map drawn after SPOT satellite images. Major faults are active since they crosscut Quaternary deposits. When their activity is not verified they appear with a dotted line. Intermediate and minor faults are not clearly active. Their relative importance is based on their associated relief and their length. Stratigraphic markers are stratigraphic layers that can be easily followed on satellite images to pick out the deformed structures. Fold traces are the contour of fold-forming rocks.